JAERI-M
93-043

ION-DRIVEN PERMEATION OF DEUTERIUM IN METALS

March 1993

Weimin SHU*, Kenji OKUNO and Yasunori HAYASHI*

日本原子力研究所
Japan Atomic Energy Research Institute

JAERI-Mレポートは，日本原子力研究所が不定期に公刊している研究報告書です。
入手の問合わせは，日本原子力研究所技術情報部情報資料課（〒319-11茨城県那珂郡東海村）あて，お申しこしください。なお，このほかに財団法人原子力弘済会資料センター（〒319-11 茨城県那珂郡東海村日本原子力研究所内）で複写による実費頒布をおこなっております。

JAERI-M reports are issued irregularly.
Inquiries about availability of the reports should be addressed to Information Division Department of Technical Information, Japan Atomic Energy Research Institute, Tokai-mura, Naka-gun, Ibaraki-ken 319-11, Japan.

編集兼発行　日本原子力研究所
印　　刷　いばらき印刷㈱

JAERI-M 93-043

Ion-Driven Permeation of Deuterium in Metals

Weimin SHU*, Kenji OKUNO and Yasunori HAYASHI*

Department of Fusion Engineering Research
Naka Fusion Research Establishment
Japan Atomic Energy Research Institute
Naka-machi, Naka-gun, Ibaraki-ken

(Received February 3, 1993)

A general model of ion-driven permeation of hydrogen isotopes at steady state is presented. In this model, new transport parameters, which not only have clear physical meanings but also contain the implanted range, are developed to distinguish the regime of ion-driven permeation at steady state. The model shows that the transport regime of ion-driven permeation depends on the incident ion flux, the thickness of membrane, the implanted range, diffusion coefficients and recombination coefficients on both sides of the membrane.

The permeation behavior of deuterium implanted into pure iron, Fe-Ti alloys and pure molybdenum are investigated. The permeation spike, permeation regime, and the effect of the incident ion energy on permeation rate are discussed.

Keywords: Permeation, Deuterium, Ion-Driven, Permeation Regime, Diffusion, Recombination, Permeation Spike, Incident Energy

---

* Kyushu University

金属中でのイオン注入による重水素透過

日本原子力研究所那珂研究所核融合工学部
舒　　衛民* ・奥野　健二　・林　　安徳*

(1993年2月3日受理)

定常状態でのイオン注入による透過過程の律速についての一般的なモデルを提出した。このモデルでは，入射飛程を考慮し，はっきりした物理的な意味のあるパラメータを導入して，定常状態でのイオン注入による透過過程の律速を識別しようとした。このモデルにより，透過過程の律速は，入射フラックス，試料の厚み，入射飛程，入射側と裏側との拡散係数と再結合係数に依存する。

イオン注入法により，純鉄とFe－Ti合金および純モリブデンにおける重水素の透過挙動を調べた。透過スパイクと透過過程の律速および透過量に及ぼす入射エネルギーの影響を議論した。

那珂研究所：〒311－01　茨城県那珂郡那珂町大字向山801－1
＊　Kyushu University

Contents

目　　次

1. Introduction

Tritium permeation through plasma facing materials is a potentially serious problem for advanced D-T reactors operating at elevated temperatures. High concentrations of tritium in the near surface region can be reached by implantation of the charge-excharge neutral flux. Because of this large concentration of mobile tritium atoms near the inner surface, a concentration gradient is established, causing tritium to diffuse into the bulk and eventually to the outer surface. Initial calculations by Wienhold et al. [1] have shown that as many as 16 g of tritium (1.6×10^5 Ci) per day could permeate through a stainless steel, INTOR (International Tokamak Reactor) - sized vessel operated at 873 K and implanted with 10^{21} $m^{-2}s^{-1}$ flux to the first wall.

To simulate the ion-driven permeation of tritium into plasma facing materials, a number of experimental investigations using hydrogen or deuterium have been made for a variety of materials, but the agreement between experiment and theory is still inadequate.

1.1. Theory consideration

1.1.1 Theory on steady state hydrogen transport

Waelbroeck et al. [2-4] developed a single transport parameter, W, which has clear physical meaning, to describe the plasma-driven permeation and recycle. However, in their model, the implanted range was not taken into account.

A steady state formalism of the ion-driven permeation has been presented by Doyle et al.[5-8]. They considered a solid membrane of thickness L with an incident ion flux of hydrogen isotope implanted to a depth r from the front surface. In steady state, incident

ion flux, Φ_i, is balanced by the flux leaving the front surface, J (recycling), and the flux leaving the back surface, Φ_p (permeation flux). These fluxes are illustrated schematically in Fig. 1. The flux balance relations are:

$$\Phi_i = J + \Phi_p \tag{1}$$

$$J = k_f C_f^2 = D\frac{C_r - C_f}{r} \tag{2}$$

$$\Phi_p = k_b C_b^2 = D\frac{C_r - C_b}{L} \tag{3}$$

where C is the concentration of hydrogen, D is the diffusion coefficient, r is the implanted range, and k is a phenomenological rate constant for molecular recombination. The subscripts f, r and b refer to the front, implanted and back planes, respectively. The same diffusion coefficients are assumed here for the front and back regions.

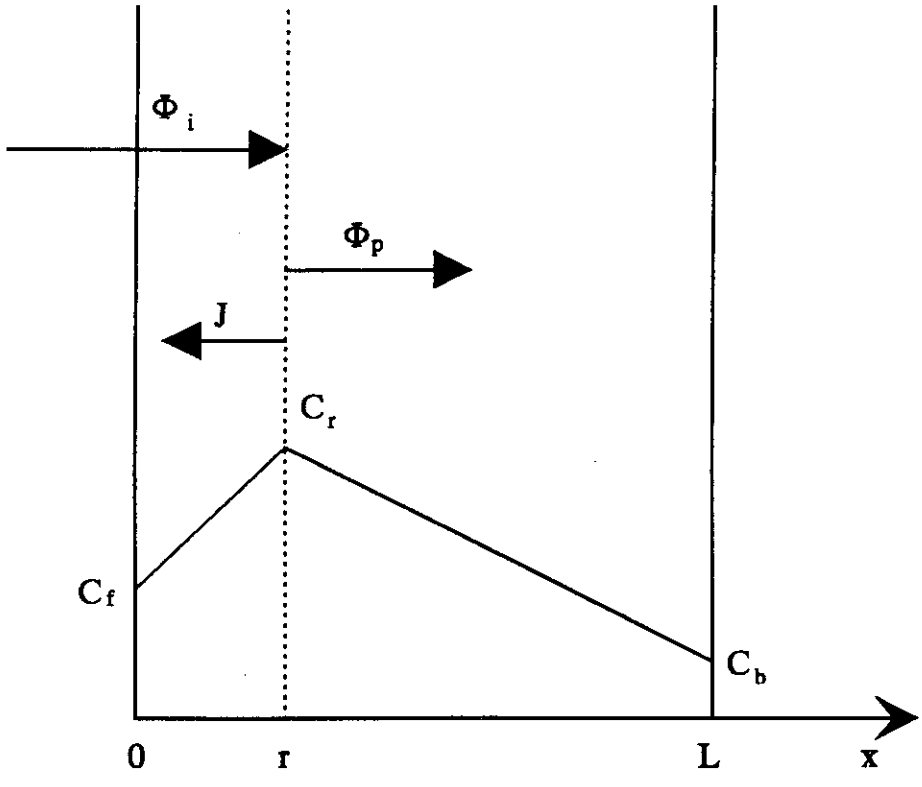

Fig. 1. A model for ion-driven permeation at steady state.

The problem then becomes one of solving Eqs. 1-3 for C_f, C_r and C_b. It is convenient to define the following dimesionless parameters:

$$u=\sqrt{\frac{k_f}{\Phi_i}}C_f\ ;\ v=\sqrt{\frac{k_b}{\Phi_i}}C_b\ ;\ \alpha=\frac{r}{L};\ \beta=\sqrt{\frac{k_f}{k_b}}\ ;\ W=\frac{r\sqrt{\Phi_i k_f}}{D}$$

Eqs. 1-3 can now be rewritten and used to form a quartic equation for v:

$$v^4+(2\alpha\beta/W)v^3+2\alpha[(\alpha/2W^2)(1+\beta^2)-1]v^2-(2\beta\alpha^2/W)v+\alpha^2(1-1/W^2)=0$$

where $\alpha<<1$.

An analytical solution to above equation was not found but a close approximation is given by:

$$v^2=\frac{\alpha(1+1/W)}{1+\alpha(1+\beta^2)(1+1/W)} \tag{4}$$

A further simplification results when $\alpha\beta^2<<W$, in which case

$$v^2=\alpha(1+1/W) \tag{5}$$

The hydrogen concentrations at x=0, r and L are determined as:

$$C_f=\sqrt{\frac{\Phi_i}{k_f}}\sqrt{1-v^2}\ ;\ C_r=\sqrt{\frac{\Phi_i}{k_f}}\beta[(W/\alpha\beta)v^2+v]\ ;\ C_b=\sqrt{\frac{\Phi_i}{k_f}}\beta v \tag{6}$$

Each of these three concentrations are plotted as a function of W in Fig. 2, where Eq. 5 was used to determine v. Sketches of the hydrogen profiles at steady state are also included as inserts in this figure. Three distinct types of hydrogen distributions result, depending on the value of W. For W>1, the profile is highly peaked at x=r and the two surface concentrations can be assumed negligible. This behavior is characteristic of diffusion-limited hydrogen transport for both the front and back sides. For $\alpha\beta^2<W<1$, $C_r \approx C_f$ and $C_b \approx 0$ indicating hydrogen recombination-determined behavior at the front surface and diffusion-limited behavior on the back side. For $W<\alpha\beta^2$ the hydrogen profile becomes uniform, which is characteristic of recombination-limited kinetics at both surfaces. Since the parameter W depends not only on material parameters (k and D) but

also on the ion implantation parameters (Φ_i and r), it can therefore be used to describe the transition from one regime to another.

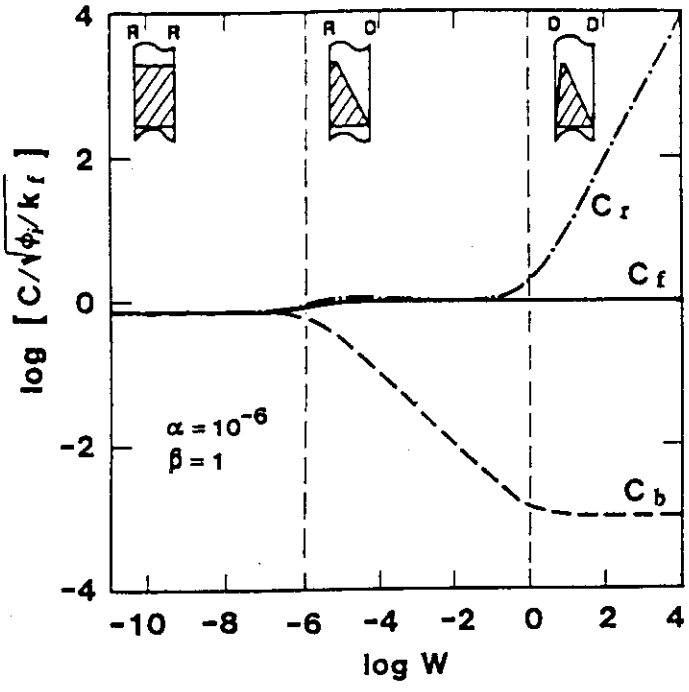

Fig. 2. Three normalized hydrogen concentrations as a function of W [5].

1.1.2. Recombination coefficient

An elementary quantity for comparing experimental results to the steady state model is the temperature dependence of the permeation rate, for which it is necessary to know the temperature dependence of recombination coefficient.

Baskes [9] developed a model to calculate the surface recombination coefficient. k is given by:

$$k = k_0 \sqrt{500 / T} \exp(-E_k / RT) \qquad (7)$$

where k_0 is a materials dependent constant, and $E_k = E_x - 2E_s$ is an activation energy for recombination which dependents on the heat of the solution for hydrogen in the material and on the activation energy for hydrogen diffusion.

The activation energy for entering the bulk, E_x, may be estimated by (E_s+E_D), the sum of the solution and diffusion activation energies for the endothermic material, and be zero for the exothermic metal in the case there is no entry barrier.

Pick and Sonnenberg [10] also derived an expression for the recombination coefficient. From their formula, k is given by:

$$k = k_0 \exp(-E_k / RT) \qquad (8)$$

where E_k=$2E_c$-$2E_s$, E_c is the activation energy for chemisorption. For clean transition metals with non-activated hydrogen chemisorption, E_c=0, the recombination rate is governed only by the heat of solution E_s. It is indicated that the surface contamination, creating an activation barrier for dissociation, effectively reduces the recombination rate.

(c) Calculation for various materials

The hydrogen diffusion coefficient and recombination coefficient are taken to have the forms [5-6]

$$D = D_0 \exp(-E_D / RT) \qquad (9)$$

$$k = k_0 \sqrt{500 / T} \exp(-E_k / RT) \qquad (10)$$

where an Arrhenis relation is assumed for D and the Baskes formula [9] is used for k.

The materials and parameters used in the calculations are listed in Table 1 [6]. Most of these parameters were taken from Wilson [11] expect for the two sets of stainless steel parameters which came from works by Braun et al. [12] (for SS-1) and Kerst [13] (for SS-2). These two data sets were chosen to span the existing data base for k in SS, which, as Wilson has noted [14], has a rather wide spread.

Table 1.

Selected values of diffusion and recombination coefficient for various materials

Material	D_0 (m^2/s)	E_D (kJ)	k_0 (m^4/s)	E_k (kJ)
α-Fe	7.8×10^{-8}	7.8	5.9×10^{-25}	-19.3
SS-1	1.8×10^{-5}	61.8	5.4×10^{-27}	65.6
SS-2	1.7×10^{-5}	58.9	2.0×10^{-24}	50.2
Mo	4.8×10^{-7}	37.6	1.6×10^{-25}	-14.5
Ni	6.9×10^{-7}	39.6	1.2×10^{-25}	24.1
Al	2.1×10^{-5}	45.3	1.2×10^{-27}	-35.7
Ti	1.8×10^{-6}	52.1	5.2×10^{-25}	94.6

The calculated transport parameter W is plotted versus reciprocal temperature in Fig. 3, assuming that the ratio of recombination coefficients $k_f/k_b=1$, the incident ion flux of $\Phi_i=10^{20}\ m^{-2}s^{-1}$ and the effective penetration ratio $r/L=10^{-6}$. The three types of hydrogen transport delineated by W are indicated on the right side of Fig. 3. It is interesting to note that for Mo, Ni, Al and SS-1 the transport is diffusion-limited on the both sides for low temperature and recombination-limited on the front side for high temperature, and that hydrogen transport in α-Fe, SS-2 and Ti is always recombination-limited on the front side and diffusion-limited on the back side in the temperature range plotted in Fig. 3.

For the parameters used for the calculation, none of the materials, including Ti, has W $<\alpha=10^{-6}$ in which case the hydrogen transport limited by recombination on both sides would occur. This fact is rather surprising because Ti reacts exothermically with hydrogen. Baskes et al. [15] proposed that permeation barriers could be used to significantly reduce the potential tritium flux through the first wall. If a permeation barrier is applied to the outer side of the wall, this effectively reduces k_b or increase β. Winter et al. [16], on the other hand, suggested that the irradiation of incident ions would produce the surface defects, which strongly increase the recombination coefficient on the front side k_f or increase β. Therefore, the assumption that $\beta=1$ seems unsuitable.

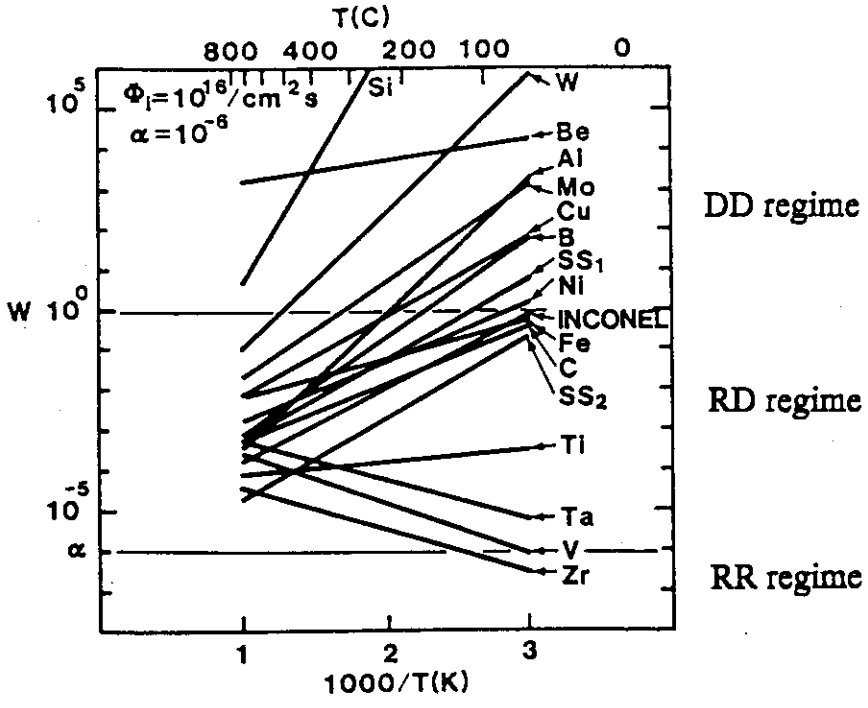

Fig. 3. Transport parameters W versus $1000/T$ for various materials [5].

1.2. Ion-driven permeation experiments

1.2.1. Permeation spike

The first ion-implantation permeation experiment was reported by Perkins and Noda [17]. They used an unanalyzed deuterium beam at energy of 15 *keV* and flux of 5×10^{18} $m^{-2}s^{-1}$ on stainless steel type 304 and 304L membranes in the temperature ranging from 740 to 950 *K*. A peculiar phenomenon, permeation spike was observed. Their experiments showed that within 20 seconds after initiating the implantation, the permeation rate reached a maximum, then decreased markedly over a time scale of about *200* seconds. The permeation spike was always the largest for the first implantation on a given sample. Causey et al. [18-19] using a 3 to 5 *keV* deuterium beam at a flux of 4×10^{19} $m^{-2}s^{-1}$ on stainless steel type 304 at 753 *K*, observed a recovery of the initial large spike after leaving the sample in vacuum overnight. Their explanation offered for the permeation spike was increase in hydrogen recombination by sputter-cleaning or chemical reduction.

Tanabe et al. [20-24] investigated the permeation behavior of deuterium implanted into a variety of materials (stainless steel, Ni, Mo, Cu and Al). They used a deuterium ion beam of energy 15~30 *keV* and flux $5\sim50\times10^{17}$ $m^{-2}s^{-1}$. The time sequence of the permeation rate showed the spike at intermediate temperatures, while the maximum permeation rate tended to be saturated at high temperature. After the appearance of the permeation spike, the permeation rate was reduced by one or two orders of magnitude. The permeation spike was explained with bulk effect. They suggested that the permeation spike was caused by decrease in bulk diffusion coefficient by migration of induced defects to deeper region than the implantation plane, or caused by diffusion enhancement by defects produced in the shallower region than implantation plane.

Winter et al. [16] using glow discharge method, observed a permeation spike for the 500 *eV* ion-implantation into pure iron at 653 *K*. The permeation spike was explained by

the increase in hydrogen recombination coefficient due to the formation of ion-induced surface defects which strongly catalyze molecular recombination. This explanation is based on the assumption that in addition to the prevailing facetted planed and steps on the multi-crystalline surface, knock-on collisions of the incident ions creates a new kinds of surface defects. Due to the distortions of the lattice and its electronic structure in their vicinity they might act as very effective recombination centers with a strongly increased local recombination rate which can overcompensate their limited number.

1.2.2. Ion energy dependence

The effect of incident ion energy on ion-driven permeation of deuterium through stainless steel type 304 has been studied experimentally by Causey et al. [25]. The permeation rate first achieved a steady state value of 3.2×10^{18} $m^{-2}s^{-1}$ for an incident ion flux of 6.8×10^{20} $m^{-2}s^{-1}$ at 20 *eV*. The bias potential was then ramped upward so that the incident ion energy increased linearly with time at the rate of 0.083 *eV/s*. The permeation rate began to decline when the ion energy reached about 40 *eV* and at 150 *eV* was only *6.2%* of the initial value. They also used Auger electron spectroscopy to relate upstream surface composition to permeation rate. The presence of either C or O on the surface resulted in a higher permeation rate than for a sputter cleaned surface.

Kerst [26] measured the permeation rates of deuterium implanted into stainless steel type 304 with two different incident ion energies at 680~710 *K*. The permeation rate approached monotonicly to steady state for low energy (20 *eV*) implantation, on the contrary, the permeation spike appeared for high energy (320 *eV*) implantation. The permeation rate at steady state for low incident energy was 700 times larger than that for high incident energy.

Winter et al. [16] used a combination of low incident energy (15 *eV*) and high energy (500 *eV*) to explore the energy dependence of ion-driven permeation through pure iron at 653 *K*. They found that the rate of IDP of hydrogen through Fe was much lower for

the high energy implantation than for low energy implantation, and that the permeation spike appeared at 500 *eV*, but not at 15 *eV*. At 673 *K*, at least one night of interruption is necessary to observe the reappearance of the permeation spike. They suggested that the incident ion energy is an important parameter for permeation rate, and that surface defects produced by the irradiation of incident ions might intervene here.

Okuno et al. [27-28] measured the dependence of incident ion energy for the permeation fluxes at steady state in the range from 100 to 1800 *eV*. The permeation rate of deuterium implanted into stainless steel type 304 decreased significantly with increasing incident ion energy in the range from 100 through 1000 *eV*, while those above 1000 *eV* little depended on the energy. In the conditions of target temperature of 790 *K* and the incident ion flux of 2.5×10^{18} $m^{-2}s^{-1}$, the permeation flux (1.4×10^{17} $m^{-2}s^{-1}$) for 100 *eV* was almost 30 times larger than that (5.0×10^{15} $m^{-2}s^{-1}$) for 1000 *eV*. On the other hand, the permeation rate of deuterium implanted into pure aluminum was almost constant for the energy of 100 to 1800 *eV* at 825 *K*, and increased gradually with increasing incident ion energy at 550 *K*.

1.2.3. Temperature inversion

Sharapov et al. [29-34] reported ion-driven permeation of hydrogen through pure molybdenum and nickel using the incident ion energy of 250 to 600 *eV*. They found that when $\ln(\Phi_p)$ was plotted against $1/T$, an inversion was seen between 710 and 860 *K*, rather than the expected linear relationship for Mo. A similar inversion occurred between 370 and 440 *K* for Ni.

Zakharov et al. [32] developed a model which holds that the inversion is due to enhanced hydrogen diffusion at low temperatures caused by interaction with mobile defects produced by the energetic implantation. The mobile defects were identified as self-interstitial atoms (SIA), which have a low migration energy. At high temperature,

these H-SIA complex decay, forcing hydrogen to diffuse in the ordinary way by hopping from one interstitial site to another.

A related result reported by Zakharov et al. [33] was obtained with a Mo membrane whose downstream side had been pre-implanted with He. Upon diffusing hydrogen through the membrane by ion-driven permeation in the temperature range where the H-SIA complexes are presumed to be stable, it was observed that the He distribution was depleted near the downstream surface. This result was interpreted as being due to the interaction between H-SIA complexes and He atoms trapped in vacancies, which resulted in some He atoms being detrapped.

1.2.4. Coatings

Hayashi et al. [35] used a hydrogen beam of energy 3 keV and flux 10^{17} $m^{-2}s^{-1}$ to investigate the effect of coating on permeation flux. The thickness of the coating film is chosen as the calculated mean range for each metal. In the steady state, the permeation flux is about 5% of the incident ion flux for the bare iron. For the specimen Pd coated onto the front surface, the permeation could not be observed, i.e., all the implanted hydrogen is absorbed in the Pd player and is re-emitted from the front surface. For the specimen Cu coated onto the front surface, large amounts of hydrogen, about 20% of the incident flux, permeate through the specimen, and for the Al coating, the permeation flux is observed to be very small.

Waelbroeck et al. [36] measured the effect of evaporating a thin film of Ti onto the front side of an iron membrane during plasma-driven permeation. There was a steady decrease in permeation flux after beginning the Ti evaporation, which leveled out at 5×10^{-3} times the value for the clean iron surface.

2. A Model for Ion-Driven Permeation at Steady State

2.1. Introduction

Ion-driven permeation (IDP) differs from gas-driven permeation (GDP) in the way by which hydrogen isotopes enter materials. In GDP, the molecules of hydrogen isotopes must be adsorbed onto the surface, dissociate there, and then move from adsorption on the surface to absorption in the bulk, resulting in a comparatively small permeation rate. In IDP, on the contrary, hydrogen isotope ions enter bulk with excess energy, resulting in a comparatively large permeation rate.

For ion-driven permeation, the permeation rate at steady state is an important measurement, since it corresponds to a surface condition similar to that expected for the plasma facing materials in a fusion device. According to the steady state model based on a delta function profile of hydrogen isotopes centered at the implanted range, the ion-driven permeation process of hydrogen isotopes can be divided into three categories depending upon the relative rate of recombination (R) and diffusion (D) on the front and back sides of the membrane, that is (1) RR regime: rate limited by recombination on both sides, (2) RD regime: rate limited by recombination on the front side and diffusion on the back side, and (3) DD regime: rate limited by diffusion on both sides.

Waelbroeck et al. [1-4] developed a single transport parameter, W, which has clear physical meaning, to describe the plasma-driven permeation and recycle. However, in their model, the implanted range was not taken into account. Doyle et al. [5-8], on the other hand, developed a different single transport parameter, W, to distinguish the regimes of ion-driven permeation of hydrogen isotopes. However, their results computed always have some arbitrariness, since the physical meaning of the parameter W and its

domain of applicability are not clear. In this work, taking the implanted range into account, we developed a couple of new transport parameters, which have clear physical meaning, to distinguish the regimes of ion-driven permeation.

2.2. Basic relations

The transport of hydrogen isotopes implanted into a membrane is schematically shown in Fig. 4. Where Φ_i is the incident ion flux, Φ_r is recycle flux (the flux of hydrogen isotope out of the front side), and Φ_p is permeation flux through the membrane (the flux of hydrogen isotope out of the back side). It is clear that for the steady state

$$\Phi_i = \Phi_r + \Phi_p \tag{11}$$

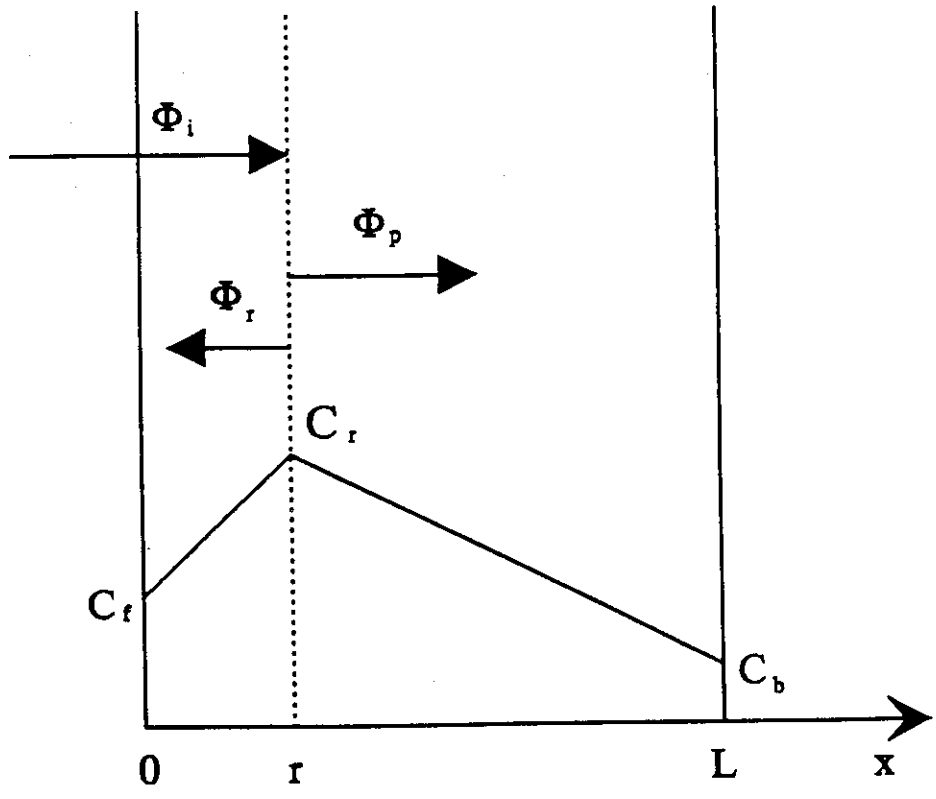

Fig. 4. A model for ion-driven permeation at steady state.

For convenience, we express Φ_p with different marks for different regimes. Φ_{RR} is the permeation flux limited by RR regime, Φ_{RD} is the permeation flux limited by RD regime, and Φ_{DD} is the permeation flux limited by DD regime.

For RR regime, because the permeation flux is recombination-limited on the back side, therefore $\Phi_{RR}<\Phi_{RD}$.

For RD regime, because the permeation flux is diffusion-limited on the back side, therefore $\Phi_{RD}<\Phi_{RR}$. On the other hand, because the recycle flux is recombination-limited on the front side, and because $\Phi_p = \Phi_i - \Phi_r$, therefore $\Phi_{RD}>\Phi_{DD}$.

For DD regime, because the recycle flux is diffusion-limited on the front side, and because $\Phi_p = \Phi_i - \Phi_r$, therefore $\Phi_{RD}<\Phi_{DD}$.

2.3. Solution of permeation flux

If the solubility of hydrogen isotopes is assumed uniform throughout the material membrane, and both diffusion coefficients of hydrogen isotopes on the front and back sides are assumed uniform (but their values may be different because the irradiation effect on the front side), the concentration, C, of hydrogen isotope implanted into a membrane of thickness of L, in one-dimensional form, can be expressed as:

$$\frac{\partial C}{\partial t} = D\frac{\partial^2 C}{\partial x^2} + S(x,t) \qquad (12)$$

where t is the time, x is the depth measured from the front side of the membrane, D is the diffusion coefficient of hydrogen isotope ($D = D_f$ on the front side, and $D = D_b$ on the back side), and $S(x,t)$ is a hydrogen isotope source term resulting from the ion-induced hydrogen isotope implantation into the membrane.

In order to substantially simplify the calculations we assume:

$$S(x,t) = S(x) = \Phi_i \delta(x - r) \qquad (13)$$

where r is the implanted range.

The boundary conditions are:

$$\Phi_r = k_f C_f^2 \; ; \qquad \Phi_p = k_b C_b^2 \tag{14}$$

where Φ_i is the flux of the hydrogen isotope out of the front side, Φ_p is the permeation flux through the membrane (the flux of the hydrogen isotope out of the back side), k is a phenomenological recombination coefficient, C is the concentration of the hydrogen isotope at surfaces, and the subscripts f and b refer to the front and back side of the membrane respectively.

The solution to Eq. 12 to Eq. 14 for $\frac{\partial C}{\partial t} = 0$ is a linear function of x and has a discontinuous first derivative (i.e. a cusp) at $x=r$. In other words, the concentration profile consists of two straight lines. As shown in Fig. 4, one line starts at C_f at the front surface and increases to C_r at $x=r$, the other line starts from C_r at $x=r$ and decreases to C_b at the back surface. If $r<<L$

$$\Phi_r = k_f C_f^2 = D_f \left.\frac{\partial C}{\partial x}\right|_{x=0} = D_f \frac{C_r - C_f}{r} \tag{15}$$

$$\Phi_p = k_b C_b^2 = D_b \left.\frac{\partial C}{\partial x}\right|_{x=L} = D_b \frac{C_r - C_b}{L} \tag{16}$$

During implantation, three transport regimes can be distinguished by the profile of $C(x)$.

(a) $C_f \approx C_r \approx C_b$:

$$\Phi_p = \frac{k_b C_b^2}{k_f C_f^2 + k_b C_b^2} \Phi_i = \frac{k_b}{k_f + k_b} \Phi_i = \Phi_{RR} \tag{17}$$

The transport is recombination limited on both the front and back sides.

(b) $C_f \approx C_r >> C_b$:

$$\Phi_p = D_b \frac{C_r}{L} = \frac{D_b}{L} \sqrt{\frac{\Phi_i}{k_f}} = \Phi_{RD} \tag{18}$$

The transport is recombination limited on the front side and diffusion limited on the back side.

(c) $C_f << C_r >> C_b$:

$$\Phi_p = \frac{D_b C_r / L}{D_f C_r / r + D_b C_r / L} \Phi_i = \frac{D_b}{D_f} \frac{r}{L} \Phi_i = \Phi_{DD} \quad (r << L) \qquad (19)$$

The transport is diffusion limited on both the front and back sides.

2.4. Two parameters

Defining $U = \frac{\Phi_{DD}}{\Phi_{RD}} = \frac{r\sqrt{k_f \Phi_i}}{D_f}$, and $V = \frac{\Phi_{RD}}{\Phi_{RR}} = \frac{D_b (k_f + k_b)}{L k_b \sqrt{k_f \Phi_i}}$, we distinguish three transport regimes. As shown in Fig. 5, when $V>1$, the system is recombination limited on both sides (RR regime); when $U<1$ and $V<1$, it is recombination limited on the front side and diffusion limited on the back side (RD regime); and when $U>1$, it is diffusion limited on both sides (DD regime).

The parameters, U and V, can therefore be used to describe the transition from RR regime to RD regime (decrease in V) and the transition from RD regime to DD regime (increase in U). The increase in membrane thickness, L, or increase in recombination coefficient on the back side, k_b, or decrease in diffusion coefficient, D_b, or increase in incident ion flux, Φ_i, will decrease the value of parameter V, thus can result in a transition from RR regime to RD regime. On the other hand, the increase in the projected range, r, or increase in the recombination coefficient on the front side, k_f, or decrease in the diffusion coefficient on the front side, D_f, or increase in incident ion flux, Φ_i, will increase the value of parameter U, thus can result in a transition from RD regime to DD regime.

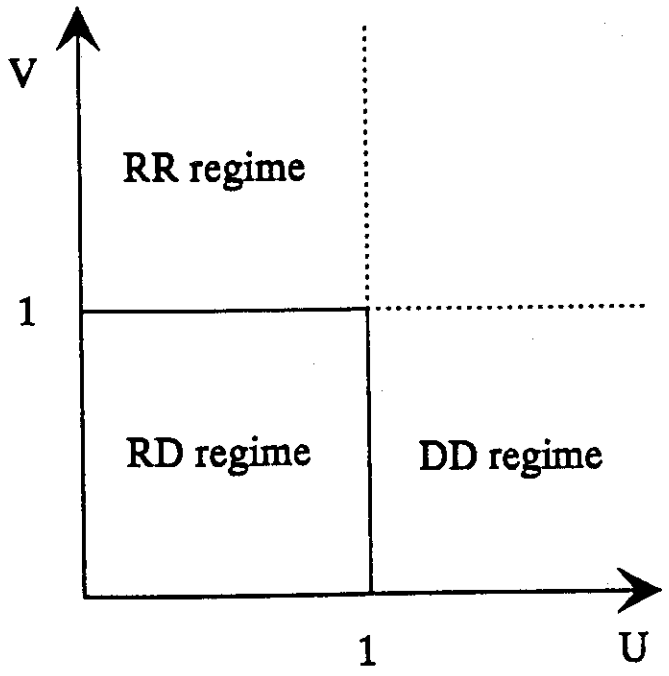

Fig. 5. Transport regimes distinguished by U and V.

Doyle et al. used one parameter, $W = \frac{r\sqrt{k_f \Phi_i}}{D}$, to distinguish the regime of ion-driven permeation [5-8], when $W < \frac{r}{L}\frac{k_f}{k_b}$, the system is recombination limited on both sides (RR regime); when $\frac{r}{L}\frac{k_f}{k_b} < W < 1$, it is recombination limited on the front side and diffusion limited on the back side (RD regime); and when $W > 1$, it is diffusion limited on both sides (DD regime).

As shown in the following, Doyle's criterion can be deduced from ours under the conditions that the diffusion coefficients are the same on both sides (i.e. $D_f = D_b = D$), and that the recombination coefficient on the front side is much larger than that on the back side (i.e. $k_f >> k_b$), Thus, $U = \frac{r\sqrt{k_f \Phi_i}}{D} = W$, and $V = \frac{Dk_f}{Lk_b\sqrt{k_f \Phi_i}} = \frac{r}{L}\frac{k_f}{k_b}\frac{1}{W}$.

Therefore, for RR regime, from $V>1$, we yield $W < \frac{r}{L}\frac{k_f}{k_b}$; for RD regime, from $U<1$ and $V<1$, we yield $\frac{r}{L}\frac{k_f}{k_b} < W < 1$; and for DD regime, from $U>1$, we yield $W>1$.

Doyle et al. [5-6] calculated the values of the parameter W, and the maximum hydrogen permeating flux, hydrogen inventory and recycle times (all as functions of W) for a variety of materials exposed to a tokamak plasma. In their calculations, the value of k_f is assumed to be equal to k_b. However, as pointed out above, Doyle's criterion and the parameter W can be used only when $k_f >> k_b$. Therefore, their results calculated always have some arbitrariness.

The recombination coefficient on the front side k_f often controls the permeation flux in IDP, and make it difficult to estimate the IDP data from the known GDP data. Experimental results have shown that k_f may increase rapidly during ion implantation, and two mechanisms have been offered for the increase in k_f. Perkins and Noda[17], and Holland et al.[18-19] suggested that increase in k_f is caused by sputtering away or chemical reduction of surface contamination. Winter et al.[16], on the other hand, suggested that increase in k_f is caused by energetic ion induced surface defects that strongly catalyze molecular recombination. Therefore, it is necessary to measure k_f itself as a function of such parameters as temperature, incident ion energy and incident ion flux. In addition, from such parameter dependence, the rate-limiting process of the transport of hydrogen isotopes in materials can be identified.

2.5. Three parameters

More generally, we take DR regime (diffusion-limited on the front side, and recombination-limited on the back side) into account. From Eq. 14 to Eq. 16 and $C_f << C_r \approx C_b$, we obtained the permeation flux by DR regime, Φ_{DR}, as:

$$\Phi_{DR} = \frac{k_b r^2 \Phi_i^2}{D_f^2} \tag{20}$$

Following the same procedure as 2.2, we give:

for RR regime, $\Phi_{DR} < \Phi_{RR} < \Phi_{RD}$;

for DR regime, $\Phi_{RR} < \Phi_{DR} < \Phi_{DD}$;

for RD regime, $\Phi_{DD} < \Phi_{RD} < \Phi_{RR}$;

for DD regime, $\Phi_{RD} < \Phi_{DD} < \Phi_{DR}$.

It is usually said that the maximum permeation flux appears in the RR regime and the minimum in the DD regime that is smaller than the maximum by several orders of magnitude [5-6, 23]. From above relations, however, we can know that only when the system is controlled by RD regime (i.e. $U<1$ and $V<1$), the permeation flux by RR regime is larger than that by RD regime (i.e. $\Phi_{RR} > \Phi_{RD}$), and the permeation flux by RD regime is larger than that by DD regime (i.e. $\Phi_{RD} > \Phi_{DD}$), and we can also know that the permeation flux by RR regime is smaller than that by RD regime (i.e. $\Phi_{RR} < \Phi_{RD}$) when it is controlled by RR regime, and that the permeation flux by DD regime is larger than that by RD regime (i.e. $\Phi_{DD} > \Phi_{RD}$) when it is controlled by DD regime.

Defining $u \equiv U = \frac{\Phi_{DD}}{\Phi_{RD}} = \frac{r\sqrt{k_f \Phi_i}}{D_f}$, $v \equiv V = \frac{\Phi_{RD}}{\Phi_{RR}} = \frac{D_b(k_f + k_b)}{L k_b \sqrt{k_f \Phi_i}}$, and $w = \frac{\Phi_{RR}}{\Phi_{DR}} = \frac{D_f^2}{r^2(k_f + k_b)\Phi_i}$, we yield: $uvw = \frac{\Phi_{DD}}{\Phi_{DR}} = \frac{D_f D_b}{r L k_b \Phi_i}$.

The parameters, u, v, and w, can be then used to distinguish the four transport regimes of ion-driven permeation of hydrogen isotopes: (1) when $v>1$, and $w>1$, the system is recombination-limited on both the front and back sides (RR regime); (2) when $uvw>1$, and $w<1$, it is diffusion-limited on the front side and recombination-limited on the back side (DR regime); (3) when $u<1$, and $v<1$, it is recombination-limited on the front side and diffusion-limited on the back side (RD regime); and (4) when $u>1$, and $uvw<1$, it is diffusion-limited on both sides (DD regime).

The transport regime of ion-driven permeation of hydrogen isotopes, therefore, depends on the incident ion flux, Φ_i, and the parameters of the front side (r, $k_f$and D_f), as well as the parameters of the back side (L, k_b and D_b). It is clear that one can transfer any regime to two other regimes by different way. For example, from RD regime, increase in u (caused by increasing Φ_i, or increasing r or k_f, or decreasing D_f) can result in a transition to DD regime, and increase in v (caused by decreasing Φ_i, or increasing D_f, or decreasing L or k_b) can result in a transition to RR regime.

2.6. Maximum concentration

Maximum potential for deleterious hydrogen-material effects, such as hydrogen embrittlement, appears at $x=r$ for ion-driven permeation at steady state, since the hydrogen concentration there is highest for all permeation regimes.

From Eq. 14 to Eq. 20, we yield:

for RR and RD regimes, $C_r = \sqrt{\frac{\Phi_i}{k_f}}$ (if $k_f >> k_b$); and for DR and DD regimes, $C_r = \frac{r\Phi_i}{D_f}$.

It is shown that the maximum concentration depends only on the incident ion flux Φ_i and the parameters of the front side, such as r, k_f , and D_f. In other words, the

parameters on the back side, such as L, k_b and D_b do not affect the maximum concentration at steady state.

2.7. Summary

A general model of ion-driven permeation of hydrogen isotopes in plasma facing materials at steady state have been developed. The transport regimes are distinguished in terms of new dimensionless parameters, either U and V, or u, v and w, which have clear physical meaning and contain the implanted range. The model shows that the transport regime of ion-driven permeation of hydrogen isotopes depends on the incident ion flux, Φ_i , and the parameters of the front side (r, k_f and D_f), as well as the parameters of the back side (L, k_b and D_b). It is also known that one can transfer any regime to two other regimes by different way if DR regime is taken into account.

3. Experimental

3.1. Apparatus

The experimental apparatus is shown schematically in Fig. 6. The apparatus consists of the following five systems: (1) an ion source for producing hydrogen isotope ion beam with variable flux and variable energy, (2) an upstream system (main chamber) for ion implantation into a target membrane, (3) a downstream system for measuring the gases permeated through the membrane, (4) a hydrogen isotope gas supply and recovery system, and (5) a vacuum pump system. The apparatus has been installed into a glovebox at the Tritium Process Laboratory (TPL) in the Japan Atomic Energy Research Institute (JAERI).

The ion source is a modification of a quartz capillary duoPIGatom ion source developed by Isoya [37]. The mass spectrometry showed that more than 90% of the ion species in the extracted beam was D^+ ion, and the rest were $D_2^+$and D_3^+ ions. The incident ion energy can be shifted from 100 to 2000 *eV*. The maximum of the ion flux implanted into the membrane ranges from 1×10^{18} D^+/m^2s at 100 *eV* to 1×10^{19} D^+/m^2s at 2000 *eV*.

The upstream side was evacuated with a cryopump (3600 *l/s* H_2, ULVAC CRYO-U10P), and the downstream side was evacuated with an ion sputter pump (80 *l/s* H_2, ULVION PST-4). The base pressure was usually kept below 2×10^{-6} *Pa* on the upstream side, and below 1×10^{-6} *Pa* on the downstream side at room temperature. The pressure on the upstream side was kept at 3×10^{-4} *Pa* during implantation.

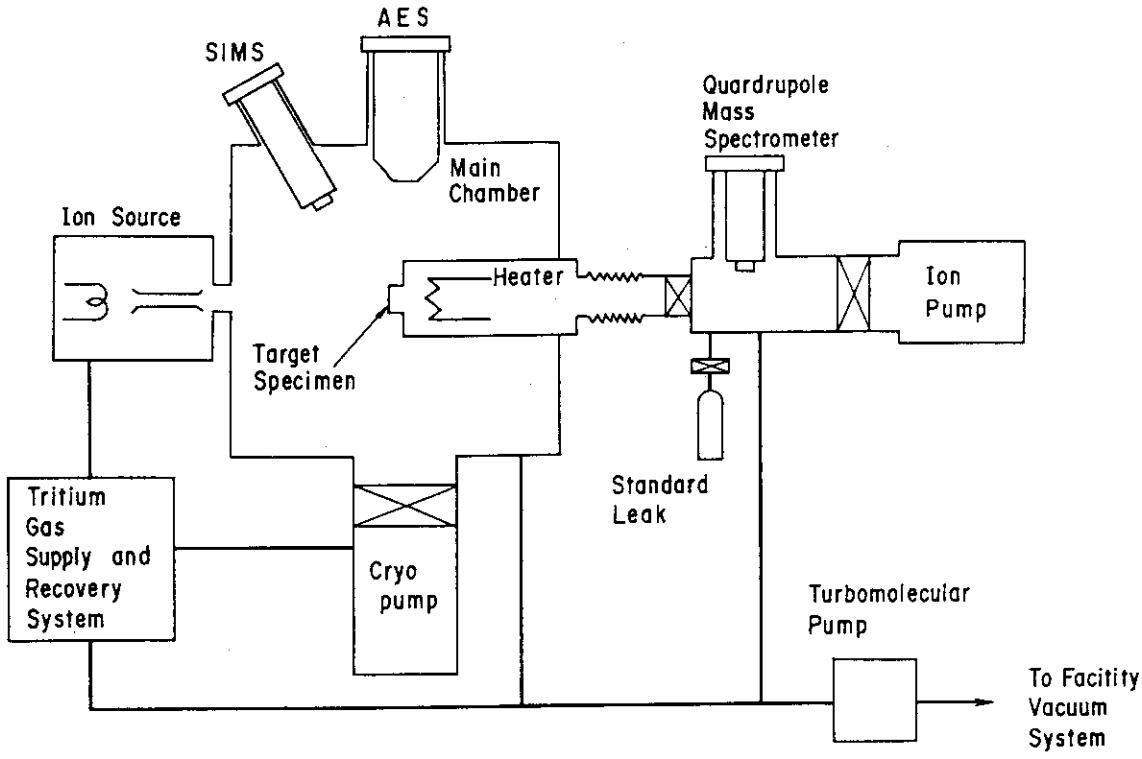

Fig. 6. The diagram of the experimental apparatus for ion-driven permeation.

3.2. Samples and procedures

The specimens used for the permeation study were disks of pure iron (99.95 wt.%Fe), Fe-Ti alloys and pure molybdenum (99.95 wt.%Mo). Specimens of Fe-Ti alloys which contain 0, 0.23, 0.64, 0.99, 1.80 at.%Ti were melted with pure titanium and commercial pure iron. The impurities in the alloys were 0.013 wt.%C, 0.01 wt.%Si, 0.16 wt.%Mn, 0.0006 wt.%S and 0.003 wt.%P.

The membranes of pure iron and Fe-Ti alloys of 3.4 *cm* in diameter were cut from foils of 0.1 *mm* thickness, and pure molybdenum membranes were cut from foils of 0.1 *mm* and 0.05 *mm* thickness. They were polished mechanically with emery papers, and then cleaned ultrasonically in acetone prior to use. A thermocouple was spot welded at the center of the membrane on the upstream side to measure the temperature of the membrane. The membrane was finally clamped to the target mounting flange of the target holder, and heated with a halogen lamp installed just behind the target membrane on the downstream side. The target holder was electrically isolated from the main chamber in order to monitor the incident ion flux implanted into the membrane. The effective implantation size of the membrane was 2.5 *cm* in diameter. The permeation flux was given from the magnitude of the mass 4 (D_2) signal of a quadruple mass spectrometer (QMS) previously calibrated by an orifice conductance method.

4. Permeation of Deuterium Implanted into Pure Iron

4.1. Permeation spike

The permeation curve for the first implantation into a virgin membrane is shown in Fig. 7. The permeation flux peaked at 4.8×10^{16} D/m^2s in 20 seconds when the previously unexposed pure iron membrane was subjected to deuterium ion beam of energy of 2000 eV and flux of 1.0×10^{19} D^+/m^2s at 413 K. The permeation flux then dropped by a factor of about 300 during the next 930 seconds. The temperature of the membrane increased 30 K while deuterium ion beam was turned on. The permeation flux decayed to the base value in about 450 seconds when the ion beam was turned off. A recovery of the initial permeation spike was observed in the first implantation after annealing the membrane at 753 K for 2 hours or leaving the membrane at about 400 K overnight. The value of the peak varied with ion energy and ion flux as well as temperature.

The permeation spike has been reported in the implantation with ion energy ranging from a few 100 eV to a few 10 keV for a variety of materials (stainless steel, Ni, Al, Mo) [17, 20-22, 27-28]. The permeation spike has not been observed at a few 10 eV ion driven implantation [25-26]. The explanations for the permeation spike emphasized the surface effect or bulk effect, that is, (1) increase in recombination coefficient on the front side (k_f) caused by sputtering away or chemical reduction of surface contamination [17, 25], (2) increase in recombination coefficient on the front side (k_f) caused by the formation of ion-induced surface defects, which strongly catalyze molecular recombination [16], (3) decrease in diffusion coefficient in back region (D_b) due to the migration of ion-induced bulk trap to the back region [20-22], and (4) increase in

diffusion coefficient in front region (D_f) due to the formation of a short diffusion path in front region [23].

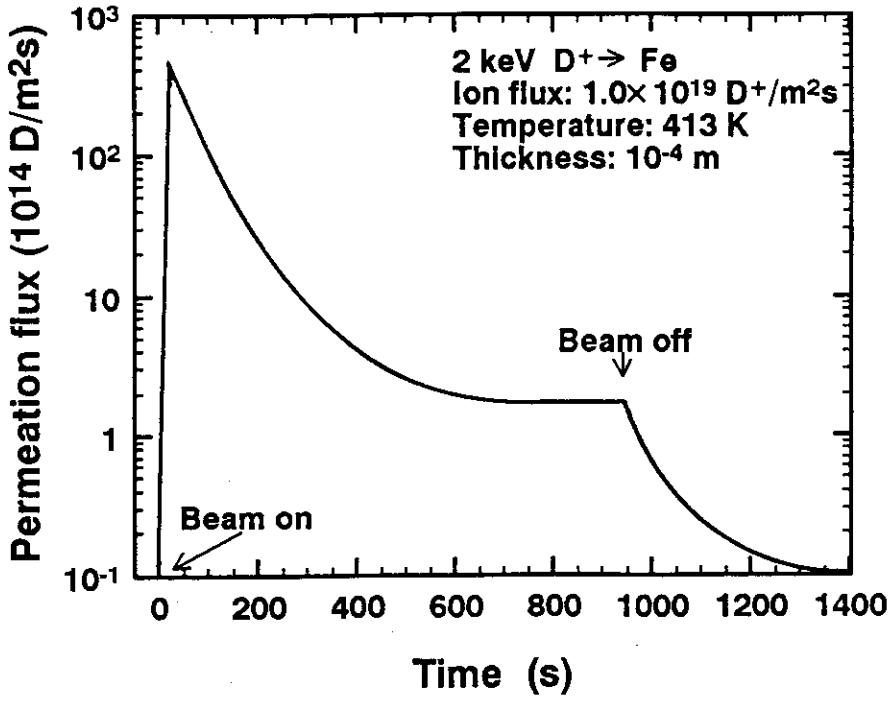

Fig. 7. The permeation curve for the implantation into a virgin membrane of pure iron (99.95 wt.%Fe).

It is improbable that the bulk effect might intervene here, since the incident ion energy used (300 to 2000 *eV*) was much lower than that used by Tanabe et al. (15 to 30 *keV*), and since the maximum of the permeation ratio was much larger than that estimated by the bulk effect hypothesis.

It is also unlikely that the surface cleaning could play an important role for this case, since the permeation spike is reproducible by thermal annealing. It seems that the permeation spike was accounted for by the surface defect hypothesis, which has been proposed by Winter et al. [16]. The microstructual model is based on the assumption that, in addition to the prevailing faceted planes and steps on the multi-crystalline surface, irradiation of the incident ions creates a new kind of surface defects. Due to the distortions of the lattice and its electronic structure in their vicinity, they might act as very effective recombination centers with a significantly increased local recombination rate. These centers should be metastable and can be annealed when the migration of the membrane atoms or defects is activated. This hypothesis can explain the recovery of permeation spike when the membrane was kept at 753 *K* for only 2 hours or at about 400 *K* for overnight.

4.2. Permeation regime

According to the steady state model based on a delta function profiled centered at the implanted range, the ion-driven permeation process of hydrogen isotopes can be divided into three categories depending upon the relative rate of recombination (R) and diffusion (D) on the front and back sides of the membrane, that is (1) RR regime: recombination on both sides, (2) RD regime: recombination on the front side and diffusion on the back side, and (3) DD regime: diffusion on both sides.

Analytical solution of the permeation flux in the steady state is listed in Table 2 for the three regimes.

Table 2

Estimation of permeation flux (Φ_p) in three regimes

RR regime	DD regime	RD regime
$\frac{k_b}{k_f + k_b}\Phi_i$	$\frac{D_b}{D_f}\frac{r}{L}\Phi_i$	$\frac{D_b}{L}\sqrt{\frac{\Phi_i}{k_f}}$

where Φ_i is incident ion flux, k is recombination coefficient, D is diffusion coefficient, subscripts f and b represent the front and back sides respectively, r is implanted range, and L is thickness of the membrane.

The dependence of permeation flux upon the incident ion flux is shown in Fig. 8. A good linear relationship was observed between the permeation flux and the incident ion flux for all cases. It is indicated that the permeation process of deuterium implanted into pure iron might belong to RR regime or DD regime.

For the incident ion energy of 1000 eV, the implanted range for implantation into pure iron was calculated to be 7.4×10^{-9} m [38], and the permeation ratio (Φ_p/Φ_i) obtained from Fig. 8 increased from 9.1×10^{-5} to 3.1×10^{-4} as temperature increased from 306 K to 535 K. If this permeation process was controlled by DD regime, D_f should be much smaller than D_b from Table 2. It could be then deduced that the trapping sites would be formed in the front region of the membrane. As shown in our previous work [39], assuming that the diffusion coefficient of hydrogen isotope in the back region is not affected by the irradiation, the permeation ratio could be rewritten for this case as

$$\frac{\Phi_p}{\Phi_i} = \frac{r}{L}\left[1+(N_t / N_l)\exp(E_b / RT)\right] \qquad (21)$$

where N_t is the number of trapping sites per volume, N_l is the number of interstitial lattice sites per volume, E_b is the trap binding energy.

It can be seen from this equation that the permeation ratio decreases with increasing temperature. However, the experimental results showed a contrary tendency. Therefore, this permeation can not be controlled by DD regime.

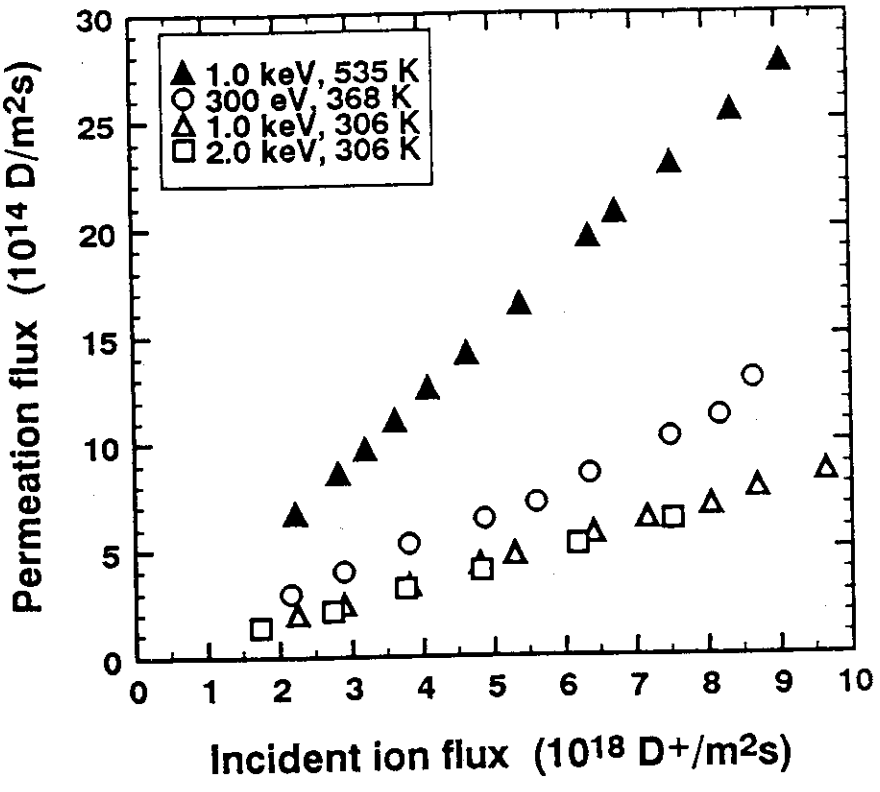

Fig. 8. The dependence of permeation flux upon the incident ion flux for pure iron (99.95 wt.%Fe).

The experimental results can be explained by RR regime, considering that the surface defects significantly catalyze molecular recombination on front site of the membrane, and that a few surface defects will be annealed when the temperature increases. The permeation ratio from Table 2 becomes in the limit $k_f >> k_b$ as:

$$\frac{\Phi_p}{\Phi_i} = \frac{k_b}{k_f} \tag{22}$$

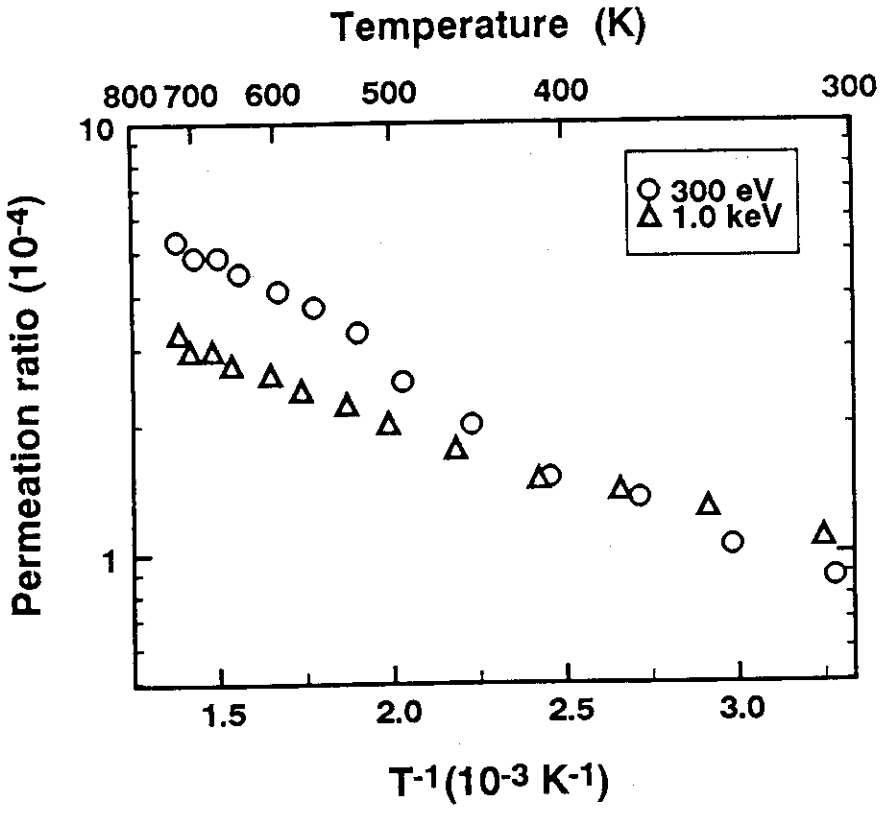

Fig. 9. Temperature dependence of the permeation ratio for pure iron.

The temperature dependence of the permeation ratio was measured in the range of 300 *K* to 800 *K*. The permeation ratios for the incident ion energy of 300 *eV* and 1000 *eV* are plotted against the reciprocal temperature in Fig. 9. The permeability of deuterium implanted into pure iron increased as temperature increased for both 300 *eV* and 1000 *eV*. The permeation ratio was found to be apparently dependent on the incident ion energy. The activation energies obtained from the curves in Fig. 9. were 8.5 *kJ/mol* for 300 *eV* and 4.7 *kJ/mol* for 1000 *eV*. Since the activation energy of recombination coefficient of hydrogen in pure iron was given as -19.2 *kJ/mol* [2], the activation energies of recombination coefficients of deuterium on the front side were obtained from Eq. 22 as -27.7 *kJ/mol* and -23.9 *kJ/mol* for 300 *eV* and 1000 *eV* respectively, supposing that the recombination coefficient of deuterium on the back side is same as that of hydrogen.

4.3. Effect of incident ion energy

It was known from the work of Causey et al. that the rate of plasma-driven permeation of deuterium through 304 stainless steel maintained constant as the ion energy increased from 20 to 30 *eV*, then began to decrease, and was only 6.2% of the initial value at 150 *eV* [25]. Kerst reported that the permeation flux at steady state for a stainless steel membrane at 680 to 710 *K* was 700 times larger at 20 *eV* than that at 320 *eV* [26]. Okuno et al. reported that the permeation flux of deuterium implanted into stainless steel type 304 for 100 *eV* D^+ ions was almost 30 times larger than that for 1000 *eV* D^+ ions at 790 *K* [27].

The effect of incident ion energy on permeation flux was investigated at an ion flux of 6.37×10^{18} D^+/m^2s and temperature of 573 *K*. In this series of experiments, a reference incident energy of 1000 *eV* (middle energy) was used in between runs at lower or higher energy to determine their effects. As shown in Fig. 10, the initial 300 *eV* run reduced permeation flux by a factor of more than 100 during 1800 seconds, indicating that the

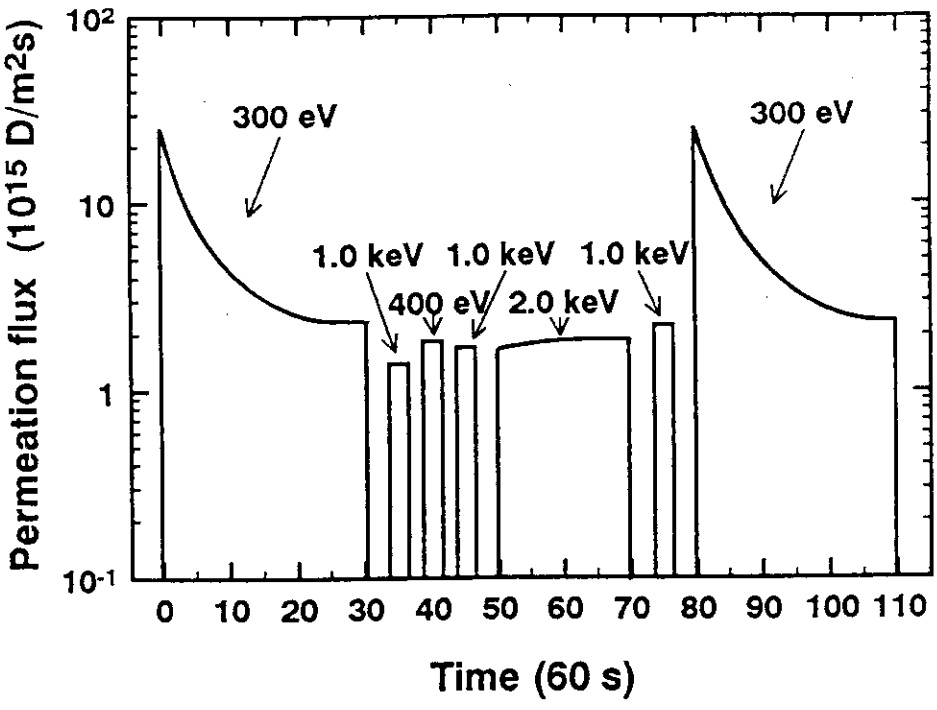

Fig. 10. Permeation history for a series of implantation into pure iron with varying ion energy.

recombination coefficient on the front side of the membrane increased by two orders, and that the achievement of the steady state of ion-driven permeation at 300 *eV* needed a long time. The first 1000 *eV* run showed a permeation flux smaller than that of 300 *eV* run and a fast achievement of steady state. The 400 *eV* run showed a permeation flux between that of 300 *eV* run and that of 1000 *eV* run. The second 1000 *eV* run showed a permeation flux between that of 400 *eV* run and that of the first 1000 *eV* run. The permeation flux for 2000 *eV* run increased gradually, indicating that the recombination coefficient on the front side of the membrane decreased gradually during the irradiation at 2000 *eV*. The third 1000 *eV* run showed a further larger permeation flux than that of the second 1000 *eV* run. The permeation flux of 300 *eV* run after a long 2000 *eV* run showed almost same tendency as that of the first 300 *eV* run, indicating that the initial surface state for the first 300 *eV* run was recovered by a long irradiation at 2000 *eV* run, and that the recombination coefficient on the front side increased by two orders during the irradiation at 300 *eV*.

In the series of experiments performed by Causey et al. [25], a reference incident flux and energy of 6.9×10^{18} D^+/m^2s and 20 *eV* were used in between runs at higher flux (7.6×10^{19} or 9.2×10^{20} D^+/m^2s) and energy (100 *eV*). Their results showed that the high energy ion removed C and O from the front surface of the SS membrane, and that this caused an increase in the recombination rate at front surface.

It was shown in Fig. 10 that the permeation flux decreased with increasing the incident ion energy, and that the higher energy run, on the contrary, would enhance the permeation flux of the following runs. It is unlikely that the surface atomic concentration was the main element under the experimental conditions, since the effect of 300 *eV* run reappeared after a long 2000 *eV* run. This suggests that the surface defects might play an important role for the permeation of deuterium implanted into pure iron at the incident energy of 300 to 2000 *eV*. The higher ion energy, the recombination centers on the front surface were more active. However, the saturation of the surface defects produced by a

long 300 *eV* (lower energy) run needed a long time, and these surface defects would join the recombination during the following runs. The permeation flux of the reference energy (1000 *eV*) run therefore increased as the surface defects produced by 300 *eV* run decreased. After a long irradiation at 2000 *eV*, the surface defects produced by 300 *eV* run were almost all replaced. These surface defects then would be formed again at the next 300 *eV* run.

4.4. Summary

For ion-driven permeation with incident ion energy of 300 to 2000 *eV*, the time sequence of the permeation flux showed a permeation spike in the first implantation into virgin or annealed membrane. It could be explained by the surface defect hypothesis. The ion-induced surface defects on the front side of the membrane acted as very active recombination centers with a significantly increased local recombination rate.

A good linear relationship was observed between the permeation flux and the incident ion flux, and the permeability of deuterium implanted into pure iron increased as temperature increased. The permeation process was controlled by RR regime. The activation energies of recombination coefficients of deuterium on front side were estimated as -27.7 *kJ/mol* and -23.9 *kJ/mol* for the incident ion energies of 300 *eV* and 1000 *eV*, respectively.

The permeation flux decreased with increasing incident ion energy, and the higher energy run, on the contrary, enhanced the permeation flux of the following runs. This suggests that the higher ion energy, the recombination centers on the front surface were more active, and that the surface defects produced by 300 *eV* (lower ion energy) run would join the next higher ion energy runs, and was almost all replaced during long 2000 *eV* (higher ion energy) run.

5. Permeation of Deuterium Implanted into Fe-Ti Alloys

5.1. Permeation regime

The dependence of permeation flux upon the incident ion flux for Fe-0.99 at%Ti is shown in Fig. 11.

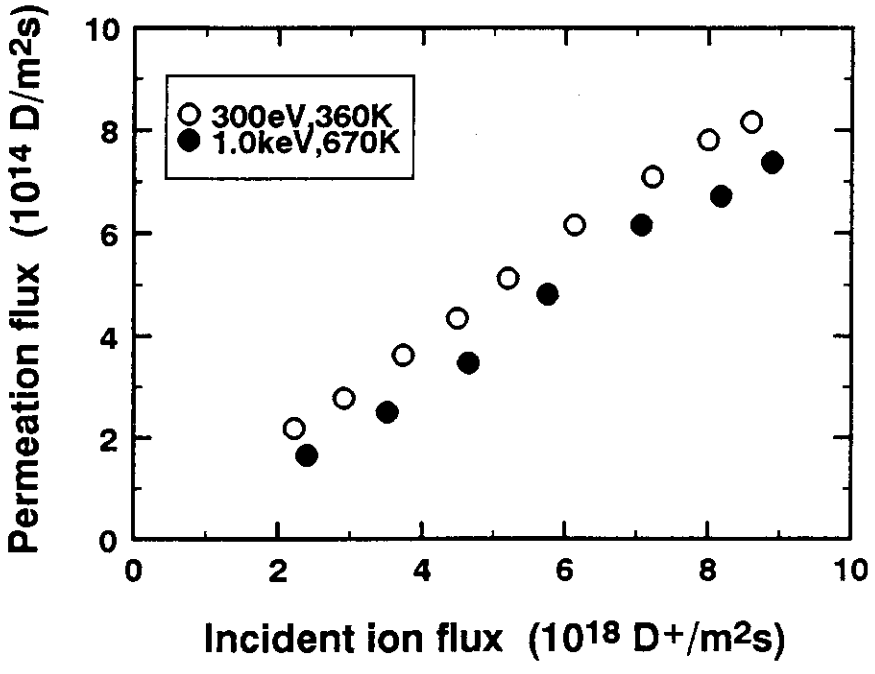

Fig. 11. The dependence of permeation flux upon the incident ion flux for Fe-0.99 at.%Ti alloy.

A good linear relationship was observed between the permeation flux and the incident ion flux for all cases. From Table 2, we can determine that if the permeation flux increases linearly with increasing incident ion flux, then this system is rate-limited by RR regime or DD regime. It is therefore indicated that the permeation process of deuterium implanted into Fe-Ti alloys might belong to RR regime or DD regime.

The temperature dependence of the permeation flux for the incident ion energy of 300 *eV* and 1000 *eV* is plotted against the reciprocal temperature in Fig. 12 and Fig. 13, respectively. The permeation flux can be easily measured for pure iron even at room temperature. For Fe-Ti alloys, on the other hand, the permeation flux can be measured only at the higher temperatures (>360 *K*), since the trapping effects in the alloys. As temperature increases, the permeability of deuterium implanted into Fe-Ti alloys increases gradually for both 300 *eV* and 1000 *eV*. The permeation fluxes are not apparently dependent on the titanium content in the alloys. However, the permeation flux of deuterium implanted into pure iron increases rapidly with increasing temperature for both 300 *eV* and 1000 *eV*.

For the incident ion energy of 300 *eV*, the implanted range for implantation into Fe-based alloys was calculated to be 2.5×10^{-9} *m* [38], and the permeation ratio (Φ_p/Φ_i) for Fe-Ti alloys obtained from Fig. 12 was about 2×10^{-4} . If the ion-driven permeation process was controlled by DD regime, since $\Phi_p/\Phi_i >> r/L$, D_f should be much smaller than D_b from Table 2. It could be then deduced that the trapping sites would be formed in the front region of the membrane. As shown in our previous work [39], the permeation ratio will decrease with increasing temperature for this case, if the diffusion coefficient of hydrogen isotope in the back region is not affected by the irradiation. However, the experimental results showed a contrary tendency. Therefore, this permeation should not be controlled by DD regime.

The experimental results can be explained by RR regime, considering that the recombination coefficient at front surface, k_f , may increase rapidly during ion

implantation. Therefore, we yield: k_f/k_b≈5000 for the Fe-Ti alloys. This ratio agree well with the work on stainless steel type 316 by Doely et al. [40].

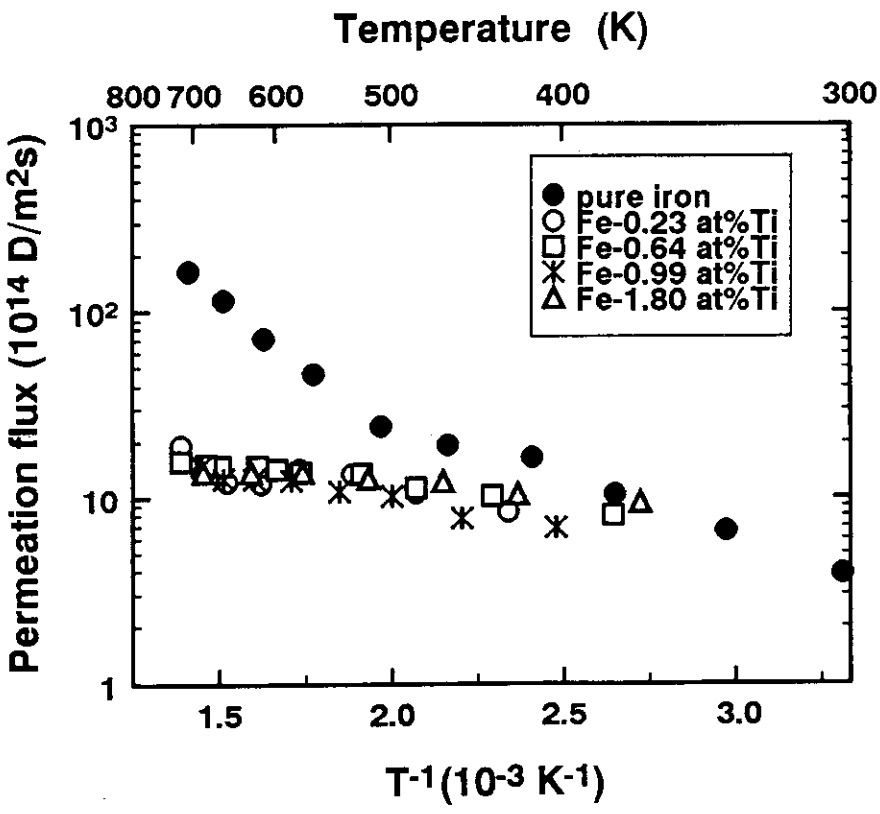

Fig. 12. Temperature dependence of permeation flux for the incident ion energy of 300 eV.

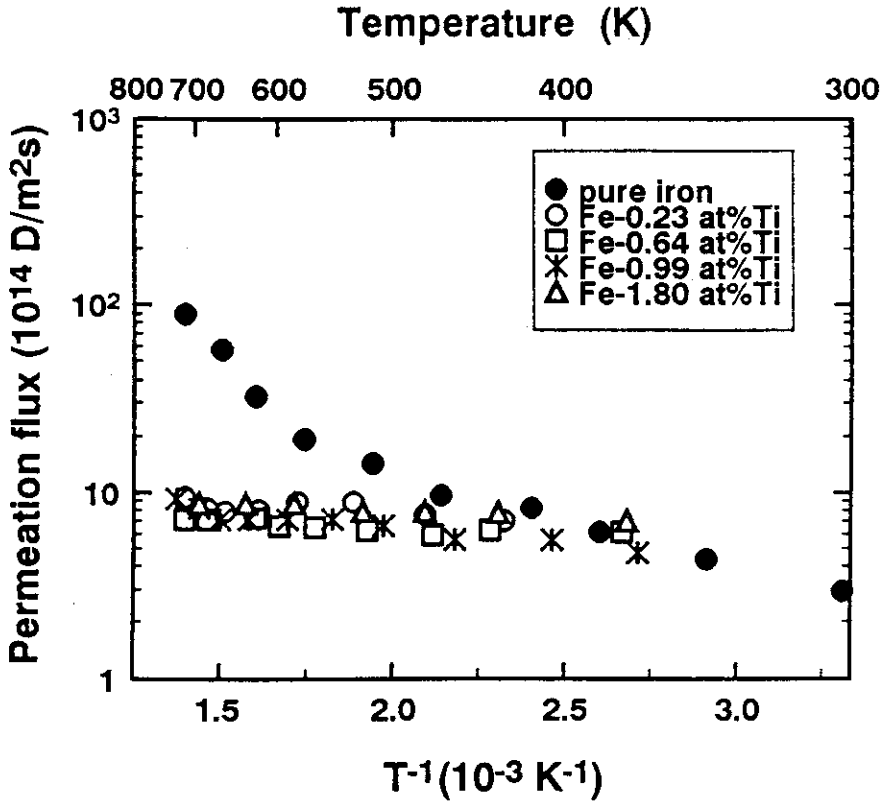

Fig. 13. Temperature dependence of permeation flux for the incident ion energy of 1000 eV.

Because the system is recombination-limited on both the front and back sides (RR regime), therefore, $v>1$, and $w>1$. Assuming that the diffusion coefficient of deuterium on the back side is almost same as that of hydrogen (about 10^{-8} m^2/s [41]), we can yield: $k_f<1.5\times10^{-18}$ m^4/s from $v>1$. This value results in $w>>1$. The recombination coefficient on the back side, k_b, for Fe-Ti alloys was then obtained as: $k_b<3\times10^{-22}$ m^4/s.

5.2. Irradiation effects

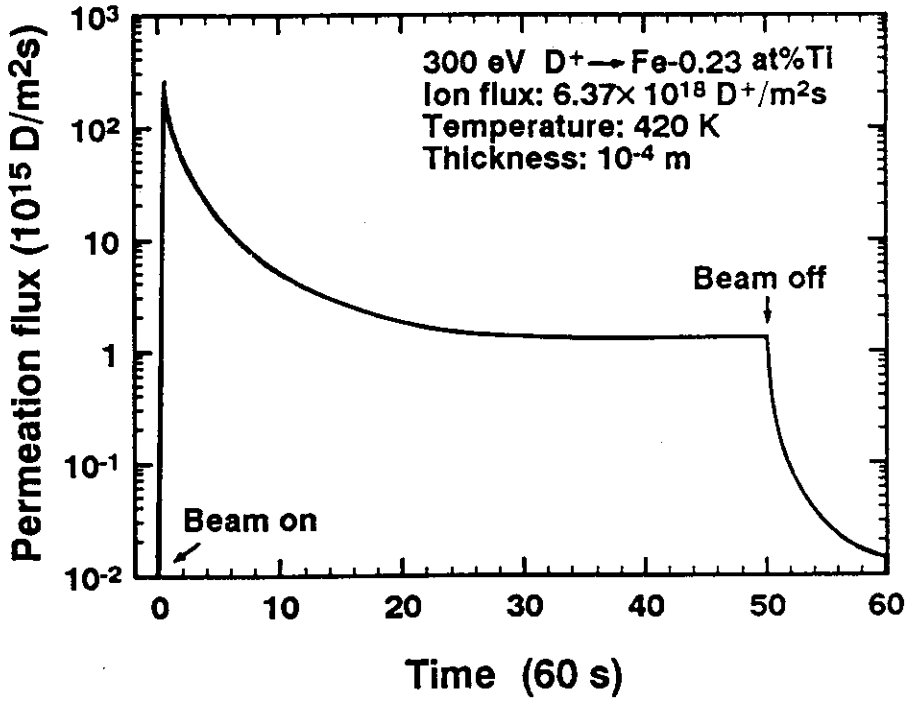

Fig. 14. The permeation curve for the implantation into the virgin membrane of Fe-0.23 at.%Ti alloy.

The permeation curve for the implantation into a virgin membrane of Fe-0.23 at%Ti alloy is shown in Fig. 14. The permeation flux peaked at 2.5×10^{17} D/m^2s in 20 seconds when the previously unexposed membrane was subjected to deuterium ion beam of energy of 300 eV and flux of 6.37×10^{18} D^+/m^2s at 420 K. The permeation flux then dropped by a factor of about 200 during the next 3000 seconds. The permeation flux decayed to base value in about 600 seconds when the ion beam was turned off. The permeation spike was observed for all the virgin or annealed membranes.

It is improbable that the bulk effect might intervene here, since the incident ion energy used (300 to 2000 eV) was much lower than that used by Tanabe et al. (15 to 30 keV) [20-22], and since the maximum of the permeation ratio was much larger than that estimated by the bulk effect hypothesis. The permeation spike is therefore almost certainly accounted for by an ion induced change in k_f.

The irradiation effects for varying incident ion energy were investigated at ion flux of 6.37×10^{18} D^+/m^2s. The dependence of incident ion energy on permeation flux was shown in Fig. 15 for Fe-0.23 at%Ti alloy at 620 K. In Fig. 15, open points and full points refer to the data obtained at the first circle (increasing the incident ion energy) and that at the second circle (decreasing the incident ion energy), respectively. The time sequences of runs 1, 2 and 3 in Fig. 15 were shown in Fig. 16. The energy dependence was also measured for other alloys and temperatures, the results showed the same tendency.

As shown in Fig. 15 and Fig. 16, the initial 300 eV run reduced permeation flux by a factor of more than 20 during 1800 seconds, indicating that the recombination coefficient on the front side of the membrane, k_f, increased by two orders, and that the achievement of the steady state of ion-driven permeation at 300 eV needed a long time. In the first circle (open points in Fig. 15), a fast achievement of steady state was obtained for 400 to 1750 eV, and as the incident ion energy increases, the permeation flux decrease for the lower incident ion energy ranging from 300 to 750 eV, then increases gradually for the higher incident ion energy ranging from 750 to 2000 eV, indicating that k_f increased

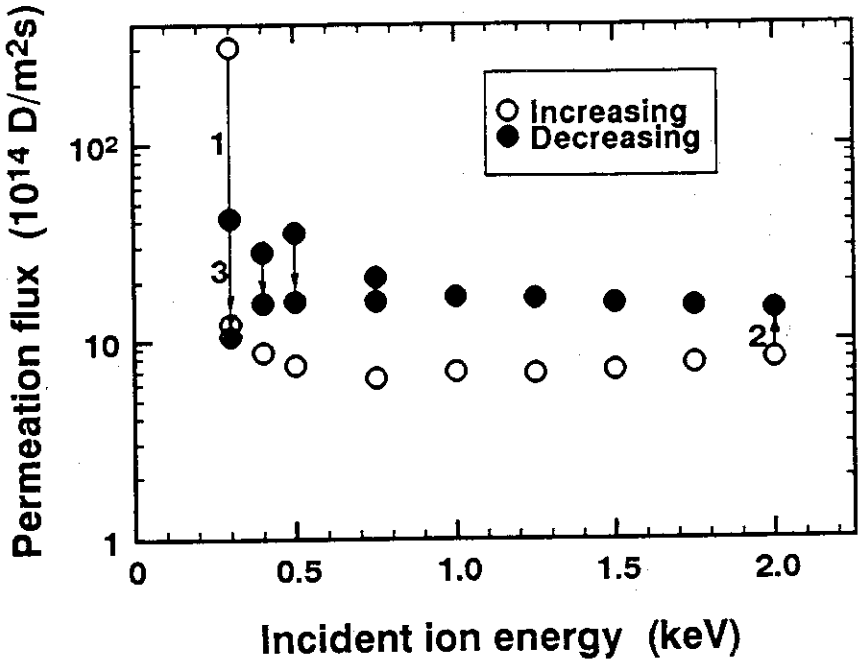

Fig. 15. The dependence of permeation flux upon the incident ion energy for Fe-0.23 at.%Ti alloy at 620 *K*.

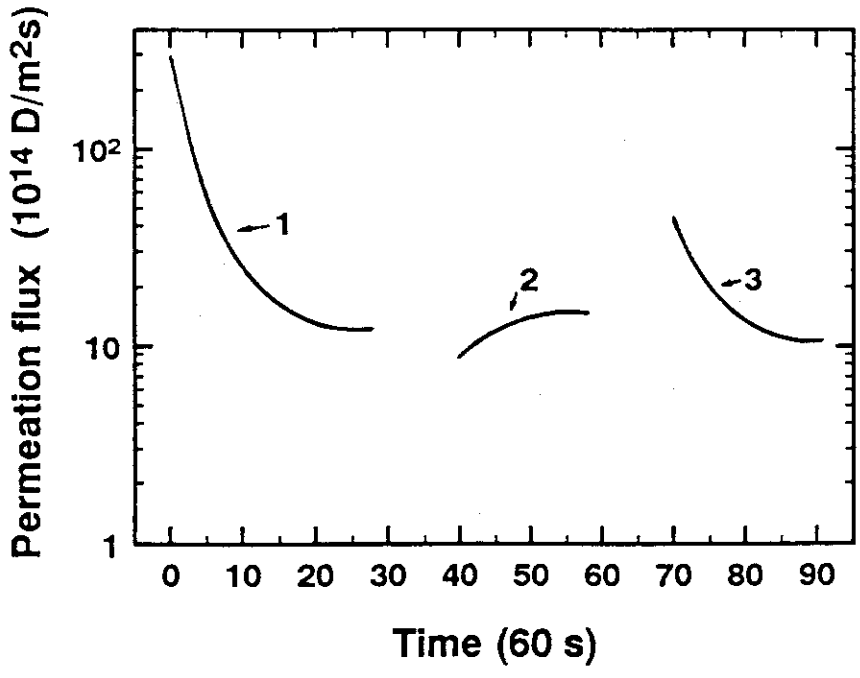

Fig. 16. The time sequences of permeation fluxes at runs 1, 2 and 3 in Fig. 15.

for the lower energy (<750 *eV*) runs, and decreased gradually during the irradiation at higher energy (>750 *eV*) runs. The 2000 *eV* run (run 2 in Figs. 15 and 16) showed a gradually increased permeation flux and slow achievement of the steady state, indicating that k_f decreased gradually during the 2000 *eV* run. In the second circle (full points in Fig. 15), as the incident ion energy decrease, the permeation flux increases gradually for the higher energy (>750 *eV*), indicating that k_f decreases gradually, and for the lower incident energy (≤750 *eV*) run, the permeation flux decreases during the irradiation, for example, the 300 *eV* run (run 3 in Figs. 4.12 and 4.13) reduced the permeation flux by a factor more than 4 during 1200 seconds.

It was shown from Fig. 15 that the permeation flux depends not only on the incident ion energy, but also on the previous irradiation. The lower energy (<750 *eV*, particularly 300 *eV*) runs reduce the permeation flux of following runs, the higher energy (>750 *eV*, particularly 2000 *eV*) runs, on the contrary, enhance the permeation flux of the following runs. It is unlikely that the surface atomic concentration is the main element for this experimental results. It seems that the irradiation effects are accounted for the surface defect hypothesis, which has been proposed by Winter et al. [16]. The microstructual model is based on the assumption that, in addition to the prevailing faceted planes and steps on the multi-crystalline surface, irradiation of the incident ions creates a new kind of surface defects. Due to the distortions of the lattice and its electronic structure in their vicinity, they might act as very effective recombination centers with a significantly increased local recombination rate. The higher ion energy, the recombination centers on the front surface are more active. However, the stable surface defects produced by lower energy (particularly 300 *eV*) runs would join the recombination during the following runs, and decrease gradually during the higher energy (particularly 2000 *eV*) runs, then increase again during the lower energy runs.

5.3. Summary

A good linear relationship was observed between the permeation flux and the incident ion flux.

The permeation flux can be easily measured for pure iron even at room temperature. For Fe-Ti alloys, on the other hand, the permeation flux can be measured only at the higher temperatures (>360 *K*), since the trapping effects in the alloys. As the temperature increases, the permeation flux increased gradually for Fe-Ti alloys, and increases rapidly for pure iron. However, the permeation fluxes are not apparently dependent on the titanium in the alloys. The permeation process can be explained by RR regime. The recombination coefficients of deuterium on the front and back sides were estimated as: k_f $<1.5\times10^{-18}$ m^4/s, $k_b<3\times10^{-22}$ m^4/s, respectively.

For ion-driven permeation with incident ion energy of 300 to 2000 *eV*, the time sequence of the permeation flux showed a permeation spike in the first implantation into virgin or annealed membrane. The permeation spike is account for by the ion-induced change in k_f.

The permeation flux depends not only on the incident ion energy, but also on the previous irradiation. The higher ion energy, the recombination centers on the front surface are more active. However, the lower energy (<750 *eV*, particularly 300 *eV*) runs reduce the permeation flux of following runs, the higher energy (>750 *eV*, particularly 2000 *eV*) runs, on the contrary, enhance the permeation flux of the following runs. It seems that the stable surface defects produced by lower energy (particularly 300 *eV*) runs would join the recombination during the following runs, and decrease gradually during the higher energy (particularly 2000 *eV*) runs, then increase again during the lower energy runs.

6. Permeation of Deuterium Implanted into Pure Molybdenum

6.1. Permeation spike

A typical permeation curve with a spike was shown in Fig. 17. The initial permeation rate peaked at about 1.5×10^{15} D/m^2s in a few seconds when a previously unexposed pure molybdenum was subjected to 2000 eV ion beam of deuterium for the incident ion flux of 8.5×10^{18} D^+/m^2s and the temperature of 440 K. The permeation rate diminished rapidly to about three fifths of the maximum in a few seconds, and then decayed gradually to the steady state value (about one fifth of the maximum) in 20 minutes. When the ion beam was turned off, the permeation rate decayed rapidly and then gradually to the base value. No permeation spike was observed, and the permeation rate at the steady state was almost same while the ion beam was turned on again. But in the first permeation after leaving the membrane remained under vacuum condition (below 3×10^{-6} Pa) at the experimental temperature overnight, the permeation rate peaked again with a smaller maximum, and then approached the same value at the steady state.

The spike effect has been explained by many researchers. Perkins and Noda [17] and Causey et al. [18-19, 25] developed a model which holds that the spike effect is due to sputtering away or chemical reduction of surface contamination. Winter et al. [16] considered that the spike effect is due to the energetic ion induced surface defects which strongly catalyzed molecular recombination. Tanabe et al. [20] emphasized bulk effect for high ion energy implantation. In their explanation, the spike effect was considered to be due to the decrease of the diffusion coefficient of hydrogen isotope in the back region caused by migration of induced defects to the deeper region than the implantation plane.

Since the spike was observed for the first implantation into the virgin or overnight membrane as noted above, it would be difficult to attribute the cause of the spike to bulk

effect considering that the incident energy used is much lower than that by Tanabe et al. It could be said that the permeation spike might be caused by either surface chemistry or surface damage, or both in this case. In order to discuss further the spike phenomenon in detail, simultaneous Auger Electron Spectrometer (AES) measurements of the membrane surface during the implantation should be required.

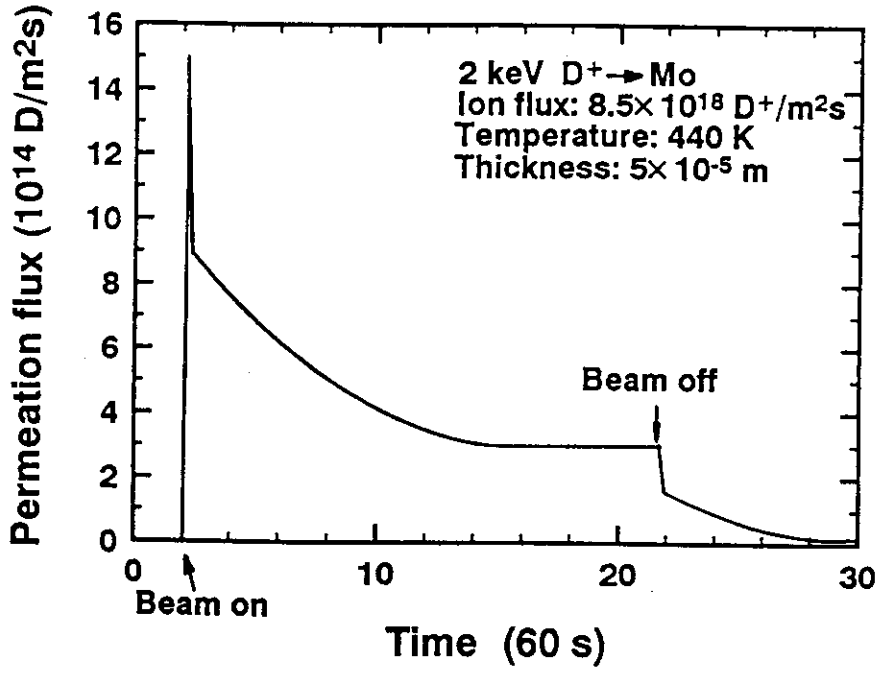

Fig. 17. A typical permeation curve with a spike for pure molybdenum.

6.2. Incident ion flux dependence

The permeation rate at steady state is an important measurement since this corresponds to a surface condition similar to that expected for first wall materials that have been exposed to a plasma in a fusion device. To investigate the permeation rate of deuterium implanted into pure molybdenum at the steady state, the dependence of the permeation rate upon the incident ion flux, experimental temperature and the incident ion energy was measured. Before the measurements, the membrane was always pre-implanted for 2 hour with 2000 eV D^+ ion beam at the incident ion flux of 8.5×10^{18} D^+/m^2s to avoid the permeation spike and prepare clear surface of the membrane.

The dependence of the permeation rate upon the incident ion flux is shown in Fig. 18 and Fig. 19 for thickness of 0.1 mm and 0.05 mm respectively. A good linear relationship was observed between the permeation rate (Φ_p) and the incident ion flux (Φ_i) for all cases. It is indicated that the permeation process may belong to DD or RR-regime. Since the permeation ratio (Φ_p/Φ_i) depends on the thickness of the membrane, the permeation process of deuterium implanted into pure molybdenum is distinguished as DD-regime due to the small diffusion coefficient of hydrogen in molybdenum. In the case of DD-regime, the permeation rate can be derived as following equation:

$$\Phi_p = \frac{D_b}{D_f}\frac{r}{L}\Phi_i \qquad (23)$$

where r is the average projected range of the implanted ions, L the thickness of the membrane, D_b the bulk diffusion coefficient of hydrogen isotope in the region deeper than r, namely the back region, and D_f that in the region shallower than r, namely the front region.

It can be also observed from Fig. 18 that as the temperature increases, the permeation rate increases for 1000 eV incident ion energy, and decreases for 2000 eV incident ion energy.

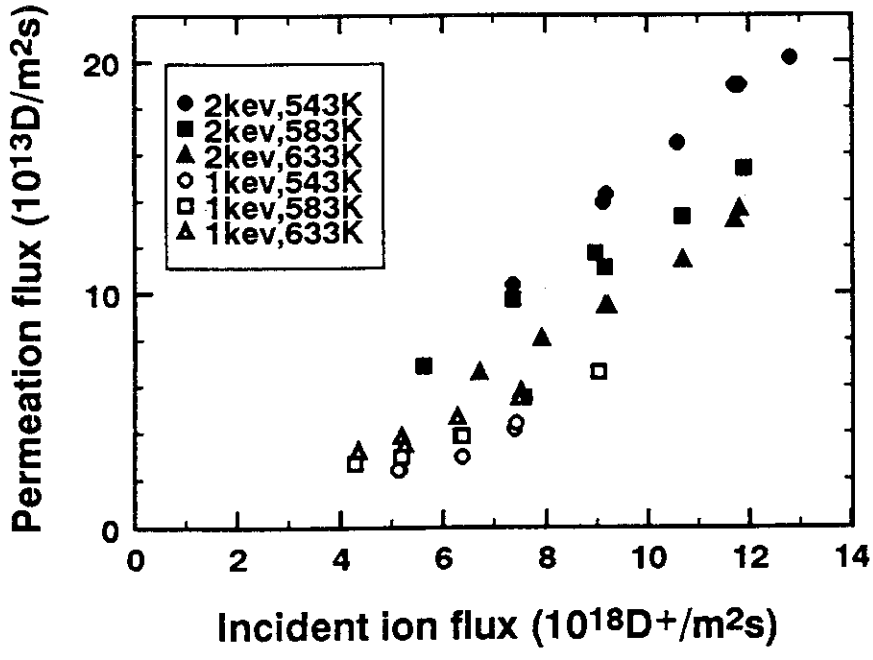

Fig. 18. The dependence of permeation flux upon the incident ion flux for molybdenum membrane of 0.1 *mm* thickness.

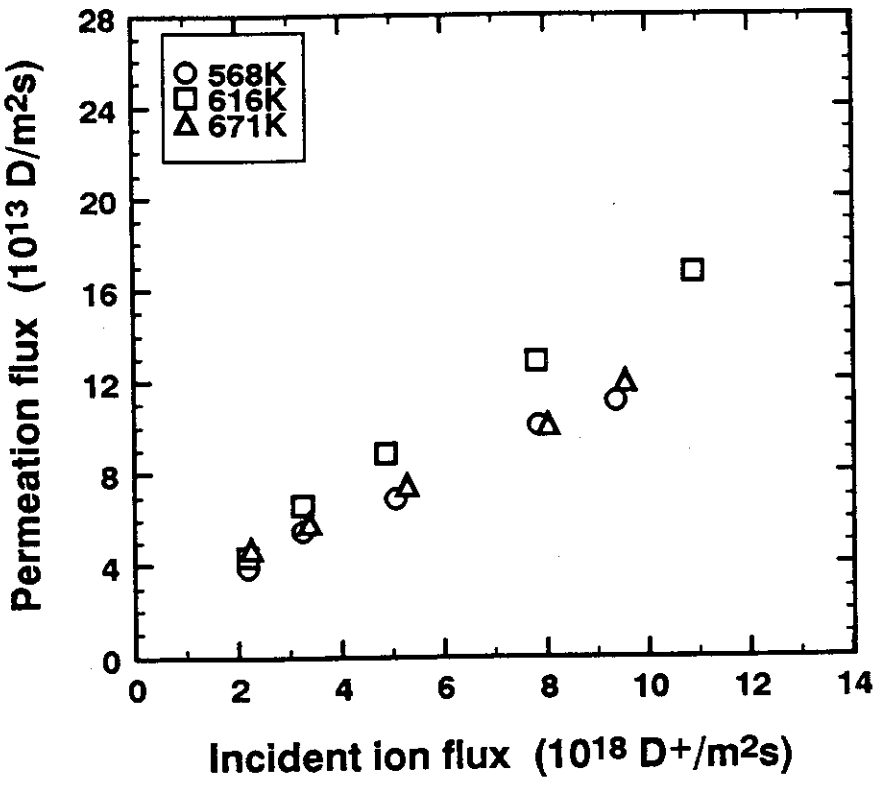

Fig. 19. The dependence of permeation flux upon the incident ion flux for molybdenum membrane of 0.05 *mm* thickness and the incident ion energy of 500 eV.

6.3. Temperature dependence

The temperature dependence of the permeation flux at the steady state was measured for the membrane of 0.05 *mm* thickness in the range from 450 to 690 *K*. The permeation fluxes for the incident ion energy of 1500 *eV* and 500 *eV* are plotted against the reciprocal temperature in Fig. 20. From this figure, the temperature dependence of the permeation flux of deuterium implanted into pure molybdenum was found to vary with the incident ion energy. For the case of 1500 *eV*, the temperature flux decreased rapidly as temperature increased in the range from 450 to 540 *K*, and became nearly constant in the higher temperature range. For the case of 500 *eV*, on the other hand, as temperature increased, the permeation flux increased rapidly in the range of 450 to 600 *K*, and decreased gradually in the higher temperature range.

This difference of temperature dependence for the different incident ion energy might be caused by the different mechanism of diffusion in the front region, since the permeation process is controlled by DD regime as noted above.

For the higher energy (1500 to 2000 *eV*), the irradiation by the implanted ions will produce the defects, which act as trapping sites for the diffusion of hydrogen isotope in the front region. If the coverage of the trapping sites is very small, the effective diffusivity of hydrogen isotope in the front region can be derived as [41]:

$$D_{eff} = \frac{D_l}{1+(N_t / N_l)\exp(E_b / RT)} \qquad (24)$$

where D_l is a lattice diffusivity, N_t the number of trapping sites per unit volume, N_l the number of interstitial lattice sites per unit volume, E_b the trap binding energy, and T absolute temperature.

Therefore, the permeation flux can be obtained as Eq. 25 from Eq. 23 and Eq. 24, assuming that the hydrogen diffusivity in the back region is not affected by the irradiation.

$$\Phi_p = \frac{r}{L}[1+(N_t / N_l)\exp(E_b / RT)]\Phi_i \qquad (25)$$

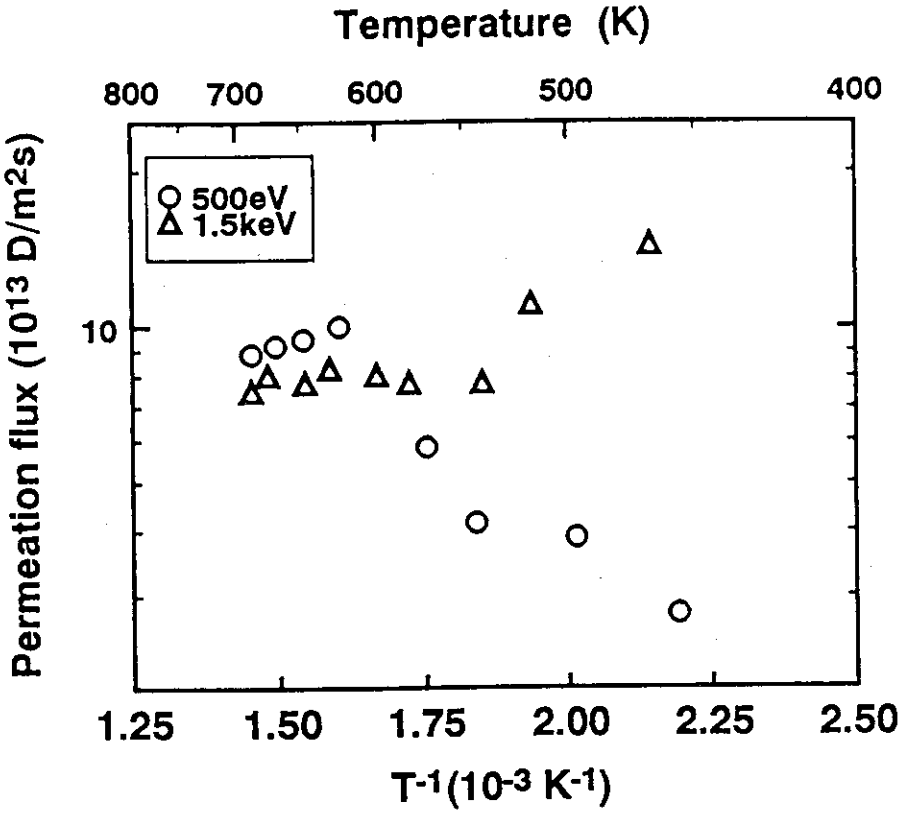

Fig. 20. Temperature dependence of permeation flux for molybdenum membrane of 0.05 *mm* thickness.

It is indicated that the permeation flux decreased with increasing temperature for the higher ion energy implantation due to the trapping effects. However, as shown in Fig. 20, the permeation became nearly constant in high temperature range from 540 to 690 K for the case of 1500 eV. According to Eq. 25, it was deduced that at high temperature the diffusion coefficient in the front region was equal to that in the back region. This suggests that the trapping sites responsible for the irradiation-reduced hydrogen diffusion in the front region at lower temperature would be annealed at higher temperature.

For the lower energy (200 to 500 eV), on the contrary, the irradiation by implanted ions would form a short diffusion path due to the production of H-SIA complexes in the front region. The self-interstitial atoms (SIA) were supposed by Zakharov et al. during the irradiation implanted into molybdenum using glow discharge method [30, 33]. The SIA were easily displaced at temperature above several tens of degree Kelvin, and had higher diffusion coefficient than did hydrogen. Since the activation energy for vacancy migration in molybdenum was substantially higher than that for migration of hydrogen (0.8 eV) [30], as shown in Fig. 21, such irradiation defects, which accelerated the diffusion of hydrogen in the front region were considered to be SIA, which migrate through the metal lattice in a dumbbell configuration with a low activation energy (about 0.2 eV). The effect of the hydrogen atom and the molybdenum atom on each other in H-SIA complex consists in the mobile molybdenum interstitial accelerating the hydrogen diffusion while at the same time the hydrogen atom itself stabilizes the SIA, increasing its lifetime and the diffusion length. As could assumed from geometric consideration, the hydrogen atom is located in the middle of the dumbbell [33].

The dissociation temperature of this dynamic complex characterizes the activation energy required to break the bond in it. Under the experimental conditions, this temperature is about 600 K, which is lower than that (727 K) by the glow discharge method [33]. At high temperature, as shown in Fig. 19, these H-SIA complexes decay, forcing hydrogen to diffuse in the ordinary way by hopping from one interstitial site to

another, and the diffusion may be reduced by some trapping sites, which were formed by dissolving of the H-SIA complexes.

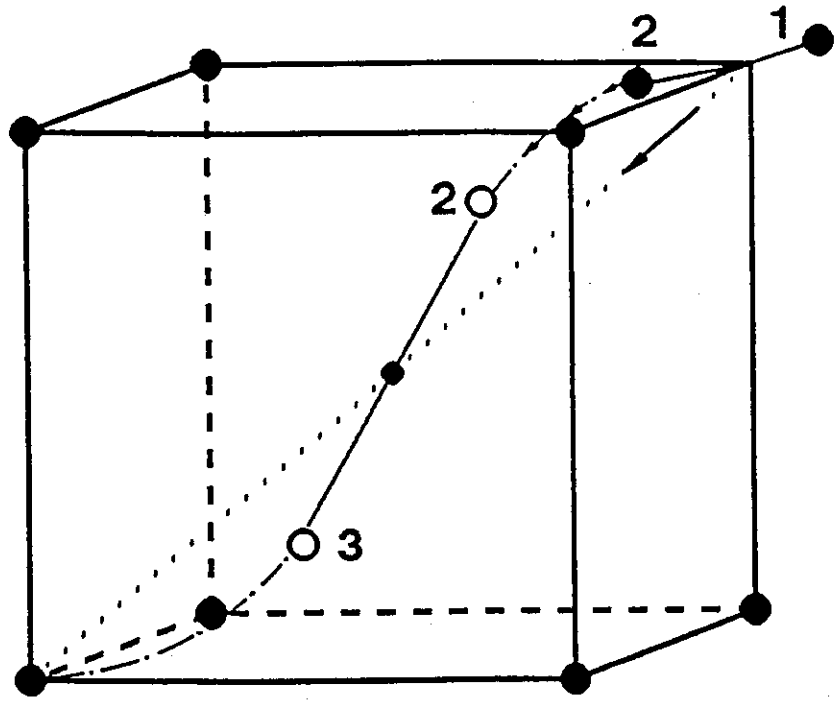

Fig. 21. Scheme of displacement of SIA-H complex in a bcc lattice.

The circle 2 and 3 denote the position of a split interstice with a hydrogen atom in the middle after a diffusion jump. Atom Mo1 occupies a lattice while Mo2 forms a new dumbbell with Mo3, which was previously at the regular lattice at the center of cube. In the jump the hydrogen atom moves along a diagonal of the cube.

6.4. Incident ion energy dependence

The incident ion energy dependence of the permeation rate at steady state was measured for the membrane of 0.05 *mm* thickness. It can be seen from Fig. 22 that the permeation rate varies with the incident ion energy and temperature, and that the temperature dependence of the permeation rate for 1500 *eV* and 500 *eV* agree well with that shown in Fig. 20.

For the higher energy (1500 to 2000 *eV*), the permeation rate increases rapidly with increasing incident ion energy at lower temperature (483 *K*), and gradually at higher temperature (568 and 616 *K*). It may be mainly caused by the trapping effect for hydrogen diffusion in the front region in lower temperature range (lower than 540 *K* for 1500 *eV* from Fig. 20), and by the implanted range r dependence at higher temperature from Eq. 25. The higher energy ions will produce more trapping sites or stronger trap binding energy, which results in lower effective diffusivity of hydrogen in the front region at lower temperature range.

For the lower energy (200 to 500 *eV*), the permeation rate increases significantly with increasing incident ion energy at lower temperature, and decreases at higher temperature. It may be mainly caused by the formation of a short path (H-SIA) for hydrogen diffusion in the front region in lower temperature (lower than 600 *K* for 500 *eV*), and by the formation of some trapping sites resulted from dissolving of the H-SIA in higher temperature range. The lower incident ion energy, the H-SIA complexes are more produced at lower temperature, and more trapping sites will be formed at higher temperature.

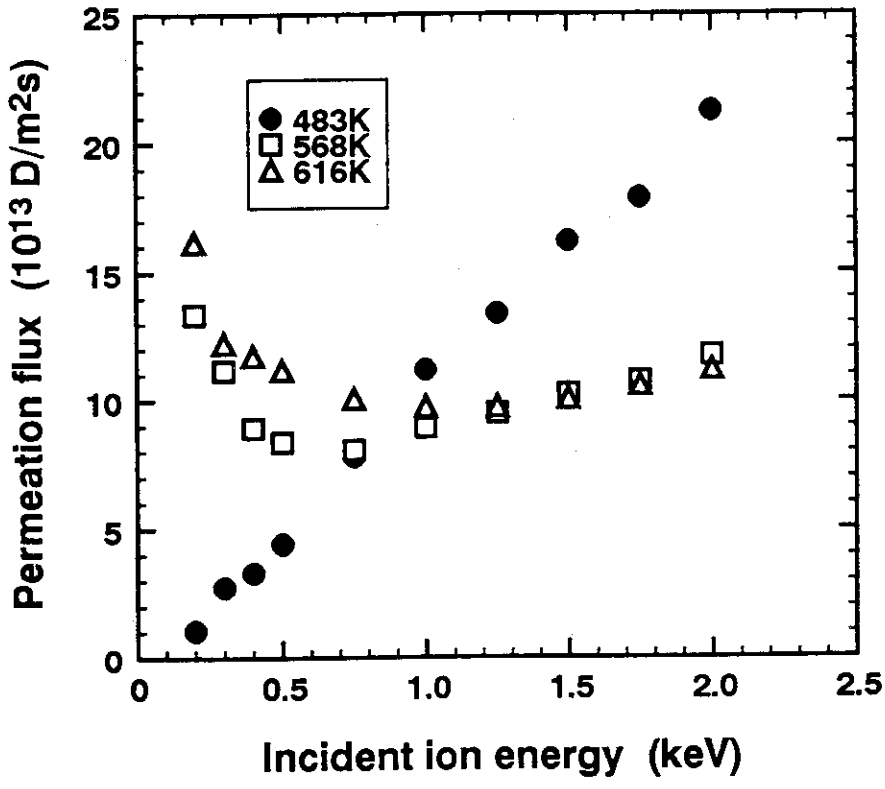

Fig. 22. The dependence of permeation flux upon the incident ion energy for molybdenum membrane of 0.05 *mm* thickness.

6.5. Summary

Implantation driven permeation behavior of deuterium through pure molybdenum has been investigated under the following conditions: (1) incident ion flux of 4~13× 10^{18} D^+/m^2, (2) membrane temperature of 450-690 K, and (3) incident ion energy of 200 ~2000 eV.

The permeation process was controlled by the diffusion of hydrogen isotope in both the front and the back regions (DD-regime).

For the case of 1500 eV, the permeation rate decreases rapidly with increasing temperature in the lower range, and become nearly constant in the higher range. It is suggested that the irradiation by 1500 eV incident ions will produce trapping sites for the diffusion of hydrogen at lower temperature, and which are annealed at higher temperature. For the case of 500 eV, as temperature increases, the permeation rate increases significantly at temperature below 600 K, and decreases gradually at temperature above 600 K. It is suggested that the irradiation by 500 eV D^+ will form a short path (H-SIA) at lower temperature, and that some trapping sites will be formed by the dissolving of the H-SIA at higher temperature.

The permeation rate increases rapidly with increasing incident ion energy at lower temperature and gradually at higher temperature for the incident ion energy ranging from 1500 to 2000 eV. It is suggested that the higher energy ions will produce more trapping sites or stronger trap binding energy at lower temperature. For the incident ion energy ranging from 200 to 500 eV, on the other hand, the permeation rate increases significantly with increasing incident ion energy at lower temperature, and decreases at higher temperature. It is suggested that the lower incident ion energy, the H-SIA complexes are more produced at lower temperature, and that more trapping sites are formed at higher temperature.

7. Conclusions

(1) A general model of ion-driven permeation of hydrogen isotopes at steady state is developed. The transport regimes are distinguished in terms of a couple of dimensionless parameters, which not only have clear physical meanings but also consist of the implanted range. It shows that the transport regime of ion-driven permeation of hydrogen isotopes depends on the incident ion flux, the parameters of the front side, and the parameters of the back sides. It is also known that one can transfer any regime to two other regimes by different way if DR regime is taken into account.

(2) For ion-driven permeation of deuterium implanted into pure iron, a permeation spike is observed for the first implantation into virgin or annealed membrane. It can be explained by the surface defect hypothesis. A good linear relationship is observed between the permeation flux and the incident ion flux, and the permeability increases as temperature increases. The permeation may be controlled by RR regime. The permeation flux decreases with increasing incident ion energy, and higher energy run, on the contrary, enhances the permeation flux of following runs.

(3) For ion-driven permeation of deuterium implanted into Fe-Ti alloys, a good linear relationship was observed between the permeation flux and the incident ion flux. The permeation flux can be easily measured for pure iron even at room temperature. For Fe-Ti alloys, on the other hand, the permeation flux can be measured only at the higher temperature (>360 *K*), since the trapping effects in the alloys. The permeation fluxes increase gradually with the increasing temperature, but are not apparently dependent on the titanium content in the alloys. The permeation process can be explained by RR

regime. The permeation flux depends not only the incident ion energy, but also on the previous irradiation. The higher ion energy, the recombination coefficient on the front side is larger. However, the low energy (particularly 300 *eV*) runs reduce the permeation flux of following runs, the higher energy (particularly 2000 *eV*) runs, on the contrary, enhance the permeation flux of the following runs.

(4) For ion-driven permeation of deuterium implanted into pure molybdenum, the permeation process is controlled by the diffusion in both the front and back sides (DD regime). The irradiation by high incident ion energy (1500 to 2000 *eV*), will produces trapping sites for diffusion of hydrogen at lower temperature, and the trapping sites are annealed at higher temperature. The higher energy ions will produce more trapping sites or stronger trap binding energy. On the other hand, the irradiation by low incident ion energy (200 to 500 *eV*), will form a shot path (H-SIA) for hydrogen diffusion at lower temperature, and some trapping sites will be formed by the dissolving of the H-SIA at higher temperature. The lower incident ion energy, the H-SIA complexes are more produced at lower temperature, and more trapping sites are formed at higher temperature.

Acknowledgments

The studies was performed at Tritium Engineering Laboratory, Japan Atomic Energy Research Institute. Sincere appreciation should be expressed to Dr. S. Shimamoto (Director of Department of Fusion Engineering Research, Japan Atomic Energy Research Institute) for his continuous support and encouragement throughout the course of this research. It is a great pleasure to thank Dr. S. Ohira (Japan Atomic Energy Research Institute) and Mr. H. Obata (Japan Atomic Energy Research Institute) for their helpful cooperation.

References

1 P. Wienhold, M. Profant, E. Waelbroeck and J. Winter, J. Nucl. Mater. 93 & 94 (1980) 866.

2 F. Waelbroeck, I. Ali-Khan, K.J. Dietz and P. Wienhold, J. Nucl. Mater. 85 & 86 (1979) 345.

3 I. Ali-Khan, K.J. Dietz, F.G. Waelbroeck and P. Wienhold, J. Nucl. Mater. 76 & 77 (1978) 337.

4 F. Waelbroeck, P. Wienhold and J. Winter, J.Nucl. Mater. 111 & 112 (1982) 185.

5 B.L. Doyle and D.K. Brice, Radiation Effects 89 (1985) 21.

6 B.L. Doyle, J. Nucl. Mater. 111 & 112 (1982) 628.

7 B.L. Doyle and D.K. Brice, J. Nucl. Mater. 122 & 123 (1984) 1523.

8 D.K. Brice and B. L. Doyle, J. Vac. Sci. Technol. A 5 (1987) 2311.

9 M.I. Baskes, J. Nucl. Mater. 92 (1980) 318.

10 M.A. Pick and K. Sonnenberg, J. Nucl. Mater. 131 (1985) 208.

11 K.L. Wilson, Nucl. Fus. Special Issue (1984) 28.

12 M. Braun, B. Emmoth, F. Waelbroeck and P. Wienhold, J. Nucl. Mater. 93 & 94 (1980) 861.

13 R.A. Kerst, J. Nucl. Mater. 103 & 104 (1981) 12.

14 K.L. Wilson, J. Nucl. Mater. 103 & 104 (1981) 453.

15 M.I. Baskes, W. Baurer, R.A. Kerst, W.A. Swansiger and K.L. Wilson, Sandia Nat. Labs. SAND81-8264 (1981).

16 J. Winter, F. Waelbroeck, P. Wienhold and T. Schelske, J. Nucl. Mater. 111 & 112 (1982) 243.

17 H.K. Perkins and T. Noda, J. Nucl. Mater. 71 (1978) 349.

18 D.F. Holland, R.A. Causey, and M.L. Sattler, Proc. Fifth Top. Meeting on the

Technology of Fusion Energy (1983) 261.

19 R.A. Causey, D.F. Holland and M.L. Sattler, Nucl. Tech./Fusion, 4 (1983) 64.

20 T. Tanabe, N. Saitoh, Y. Etoh and S. Imoto, J. Nucl. Mater. 103 & 104 (1981) 483.

21 T. Tanabe, Y. Yamanishi, K. Sawada and S. Imoto, J. Nucl. Mater. 122 & 123 (1984) 1568.

22 T. Tanabe, Y. Furuyama and S. Imoto, J. Nucl. Mater. 122 & 123 (1984) 1563.

23 T. Tanabe, Y. Furuyama and S. Imoto, J. Nucl. Mater. 145-147 (1987) 305.

24 T. Tanabe, M. Takeo and S. Imoto, J. Nucl. Mater. 185 (1991) 286.

25 R.A. Causey, R.A. Kerst and B.E. Mills, J. Nuc. Mater. 122 & 123 (1984) 1547.

26 R.A. Kerst and W.A. Swansiger, J. Nucl. Mater. 122 & 123 (1984) 1499.

27 K. Okuno, S. Ohira and Y. Naruse, Fusion Technol. 19 (1991) 1607.

28 T. Hayashi, K. Okuno, K. Yamanaka and Y. Naruse, J. Alloys and Comp. (1992) (in press).

29 V.M. Sharapov, A.P. Zakharov and V.V. Matveev, Sov. Phys. Tech. Phys., 20 (1976) 1262.

30 V.M. Sharapov and A.P. Zakharov, Sov. Phys. Tech. Phys. 21 (1976) 351.

31 V.M. Sharapov and A.P. Zakharov, Sov. Phys. Tech. Phys. 23 (1978) 678.

32 A.P. Zakhrov, A.E. Gorodetsky and V.M. Sharapov, Z. Phys. Chem. Neue Folge (1979) 825.

33 A.P. Zakharov, V.M. Sharapov and A.E. Gorodetsky, Sov. Phys. Dokl. 25 (1980) 309.

34 V.M. Sharapov, A.I. Pavlov and A.P. Zakharov, Russ. J. Phys. Chem. 56 (1982) 730.

35 Y. Hayashi, A. Tahara and M. Ishibashi, Hydrogen Effects on Material Behavior, Edited by N.R. Moody and A.W. Thompson, 1990, 11.

36 F. Waelbroeck, K.J. Dietz, P. Wienhold, J. Winter, I. Ali-Khan, H. Merkens and E. Rota, J. Nucl. Mater. 93 & 94 (1980) 839.

37 A. Isoya, Helv. Phys. Acta, 59 (1986) 632.

38 K. Sone, JAERI-M6293 (1975).

39 W.M. Shu, K. Okuno, Y. Hayashi, S. Ohira and Y. Naruse, Fusion Technol. 21 (1992) 1934.

40 B.L. Doyle and D.K. Brice, J. Nucl. Mater. 145 - 147 (1987) 288.

41 W.M. Shu, Y. Hayashi and A. Tahara, J. Less-Com. Met. 173 (1991) 740.